Evolution of the soot particle size distribution along the centreline of an n-heptane/toluene co-flow diffusion flame

Jochen A.H. Dreyer[a,b,e], Maximilian Poli[a], Nick Eaves[a], Maria L. Botero[c], Jethro Akroyd[a,e], Sebastian Mosbach[a,e], Markus Kraft[a,d,e,*]

[a] *Department of Chemical Engineering and Biotechnology, University of Cambridge, Philippa Fawcett Drive, Cambridge, CB3 0AS, United Kingdom*
[b] *CoaST, Department of Chemical and Biochemical Engineering, Technical University of Denmark (DTU), Building 229, 2800, Kgs. Lyngby, Denmark*
[c] *Department of Mechanical Engineering, National University of Singapore, 9 Engineering Drive, 117576 Singapore*
[d] *School of Chemical, and Biomedical Engineering, Nanyang Technological University, 62 Nanyang Drive, 637459 Singapore*
[e] *Cambridge Centre for Advanced Research and Education in Singapore (CARES), CREATE Tower, 1 Create Way, 138602 Singapore*

Abstract

A newly developed experimental set-up for studying liquid hydrocarbon combustion in the well-established Yale burner was used to investigate the correlation between fuel composition and its sooting propensity. Soot particle size distributions (PSDs) and flame temperatures along the centreline of an n-heptane/toluene co-flow diffusion flame are reported. The results are compared to soot temperature and volume fraction profiles obtained using colour ratio pyrometry. The addition of toluene (0, 5, 10, and 15 mol%) to heptane moved soot inception to lower heights above the burner (HAB). The earlier inception extended the soot growth zone in the toluene-laden flames, leading to larger soot primary and agglomerate particles. Toluene addition had little influence on the maximum soot number density, indicating that the observed increase in soot volume fraction can mainly be attributed to the increase in particle size. The reported PSDs inside a vapour-fed diffusion flame are the first of their kind and provide a comprehensive dataset for future studies of combustion chemistry and soot particle models.

Keywords: Soot, laminar diffusion flame, liquid fuel, toluene/heptane, particle size distribution, colour-ratio pyrometry

*E-mail: mk306@cam.ac.uk

1. Introduction

Soot formed by incomplete combustion of hydrocarbons has adverse effects on human health [1] and is a major contributor to anthropogenic climate change [2–4]. However, useful carbonaceous particles such as carbon black are also prepared through combustion on an industrial scale and are used as rubber filler for tire reinforcement [5], additive for electrically conductive polymers [6], or electrode material in batteries [7, 8]. The aim of soot research is to gain a fundamental understanding of the chemical reactions, inception process and PAH clustering, and soot growth leading to soot formation in practical applications. Such an understanding could then be used to mitigate soot emission and enhance the efficiency during energy conversion (internal combustion engines, jet engines, gas turbines, etc.) or to produce tailor-made carbonaceous nanoparticles for industrial applications. In this context, investigating soot formation in laminar flames using aliphatic and aromatic fuel mixtures encountered in real combustion systems is an important area of research [9–11].

Traditionally, soot research in laminar flames has focused on gaseous fuels because they are easy to handle, with ethylene being amongst the most common choices [12–15]. In order to study more realistic fuels, less sooty methane flames have been used and doped with small amounts of aromatics and aliphatics [16, 17]. This approach was used to quantify the sooting propensity of a range of aliphatics [16], aromatics [18], and oxygenated [19, 20] fuels by measuring the maximum soot volume fraction inside the doped methane flame. The maximum soot volume fraction can hereby be measured using laser-induced incandescence [18–20] or flame pyrometry [16, 17, 21] and converted into apparatus-independent yield sooting indices (YSIs) [20]. McEnally and Pfefferle [22] also doped five different one-ring aromatics (benzene, toluene, ethylbenzene, styrene, phenylacetylene) into a methane diffusion flame and illustrated the importance of the side chain attached to the phenyl ring (H, CH_3, $CH{=}CH_2$, or $C{\equiv}$ CH). Their experiments indicated that the naphthalene concentration and soot volume fraction are proportional, making naphthalene formation a crucial step in polycyclic aromatic hydrocarbon (PAH) growth from aromatic fuels under the studied experimental conditions [22]. Other researchers linked the amount of key species (benzene, pyrene, acetylene) to the onset and rate of soot inception [23]. Differences in the type and quantity of such species ultimately reflected in the soot number density and size of the soot particles [23–25]. Adding aromatics such as *n*-propylbenzene to *n*-dodecane/methane diffusion flames was reported to

result in earlier soot inception and increased soot number densities [26]. Similarly, the addition of toluene to a methane diffusion flame caused a significant increase in the soot volume fraction compared to n-heptane addition [25].

Research on pure liquid fuel combustion is less common, partly due to experimental difficulties. One of the simplest set-ups to study liquid fuels is the wick-fed diffusion flame. Such flames have mainly been used to measure smoke points of fuels to assess the fuel's sooting propensity and to calculate apparatus-independent sooting indices, such as the threshold soot index (TSI) [27] or oxygen extended sooting index (OESI) [28]. Using wick-fed flames to measure smoke points is the standard method for characterising kerosine and aviation turbine fuel as specified in ASTM Standard D1322-15e1. This methodology was used to study sooting propensity of fuel surrogates such as heptane and toluene [24, 29] or oxygenated diesel additives such as polyoxymethylene dimethyl ethers [11]. In addition to sooting propensities, this flame was used to measure particle size distributions (PSD) as a function of fuel flow rate using a differential mobility spectrometer and hole-in-tube probe for sampling [24, 29]. The probe design did not allow sampling from within the flame but an increased mean particle size was observed at the flame tip when toluene was added to the wick-fed heptane flame [24]. More recently, a premixed flat flame was fed with pre-vaporised heptane/toluene and PSDs were measured using the burner stabilised stagnation (BSS) approach [23]. Hereby, the hole-in-tube sampling line is incorporated into the stagnation plate, enabling the sampling of stagnation flames with minimal flame perturbation [30]. The study showed that in premixed flames containing toluene, soot nucleation starts earlier while larger soot particles and volume fractions were detected in the heptane fed flame [23]. One drawback of the BSS is that the soot evolution from the burner surface to the stagnation point can not be studied. Only information about the soot at the stagnation point is retrieved. However, there remains a lack of experimental data in well-defined laminar flames using more realistic fuels such as pre-vaporised heptane as also recognised during the International Sooting Flame (ISF) workshop 2018 [31]. Having PSDs inside such flames would further extend the recent efforts to simulate PSDs in ethylene-fed BSS flames [32–34] to more realistic fuel surrogates.

The **purpose of this study** is to provide a comprehensive dataset of soot PSDs (as opposed to averaged sizes or volume fractions) inside a well-defined liquid-fueled co-flow diffusion flame. Four different fuel mixtures containing n-heptane and toluene were studied to evaluate the influence of aromatics on the evolution of particle size and number along the centreline of the flame. The soot was sampled using a newly developed quartz probe that facilitated the monitoring of the entire soot evolution process, starting with soot nucle-

ation, followed by growth, aggregation and agglomeration, and finally soot oxidation. Colour ratio pyrometry was applied to compare the PSDs to soot volume fractions and to assess the flame pertubation caused by the intrusive sampling. The presented experimental results explain why toluene has a higher sooting propensity and how it reflects in the PSD and soot volume fraction evolution. The PSD dataset is attached in the supporting information to provide a reference for the soot community and to test the various soot particle models used in literature [32–37].

2. Materials and methods

2.1. Co-flow diffusion flame

A new experimental flame set-up was developed to study vapour-fed co-flow diffusion flames (Fig. 1a). A syringe pump (New Era NE-501) delivered 7 g h^{-1} of fuel to an evaporator (Bronkhorst CEM). Here, the fuel was mixed with 0.2 SLPM Ar (Bronkhorst El-Flow) and evaporated. The fuel/carrier gas mixture was passed through heated lines (150 °C) to the central 1/4" stainless steel tube (inner diameter 0.218") of a Yale burner [17, 21]. Room temperature compressed air at 50 SLPM (Bronkhorst El-Flow) was used for the co-flow through a 3" stainless steel honeycomb mesh (0.017" wire diameter, 18x18 mesh). The burner was mounted on a vertical translational stage (Festo) with a positioning accuracy of 0.1 mm.

In this study, four different fuel mixtures (pure *n*-heptane, and 5, 10, and 15 mol% toluene in heptane) were used. The required volumetric quantities of *n*-heptane (VWR, 99.8 %) and toluene (Sigma-Aldrich, 99.8 %) were calculated based on the desired mol% composition. The densities of the mixtures required for the syringe pump were determined experimentally by measuring the mass of a known volume of fuel.

2.2. Flame temperature

The flame temperatures were measured with an S-type thermocouple having a wire diameter of 0.2 mm and microscopically measured bead size of 0.6 mm. Two pull-action computer-controlled solenoids enabled the rapid insertion and removal of the thermocouple to/from the flame. Temperatures were measured over 60 s to detect the height above the burner (HAB) at which soot starts to form. In the presence of soot, the deposition of soot on the thermocouple causes the measured temperature to decrease over time due to an increasing emissivity and bead size [38]. After each temperature measurement, the thermocouple was placed above the flame tip to burn off any soot deposits. To avoid underestimation of the thermocouple junction temperature T_j due to soot deposition, a linear extrapolation to $t = 0$ s was

used for T_j [38, 39]. The junction temperature was corrected for radiation to obtain the gas temperature T_g [40]:

$$T_\mathrm{g} = T_\mathrm{j} + \epsilon_\mathrm{j} \cdot \sigma \frac{(T_\mathrm{j}^4 - T_\mathrm{w}^4)d}{k \cdot Nu} \tag{1}$$

The temperature dependant junction emissivity ϵ_j was calculated with the reported cubic polynomial for S-type thermocouples [40] while Nu was calculated for a cylindrical profile [41]. T_w is the ambient temperature, σ is the Stefan-Boltzmann constant, and k is the thermal conductivity of the gas. The mapping of the centreline temperature was repeated 7 times and calculated gas temperatures were averaged. The uncorrected junction temperatures T_j can be found in the Supporting Information (Fig. S2).

2.3. Soot particle size and number

Soot samples from flames are most commonly taken with a hole-in-tube probe, i.e., a stainless steel tube having a small orifice to draw in a sample [42–46]. Previous studies have used such probes to sample soot from the flame tip as well as from within flames, and risk significantly perturbing the flame with respect to the flow field and temperature profile [45, 46]. In this study, a newly developed sampling probe based on the report by Hepp and Siegmann [47] was used to take soot samples from within the flame. Advantages over the hole-in-tube approach are a reduced flame disturbance when sampling from within the flame and that the probe geometry induces enhanced mixing between the sample and diluent [47, 48]. Except the quartz tube, all parts required for assembling the sampling probe are standard fittings. A technical drawing of the design as well as the part numbers of the used fittings are provided at the end of the supporting information.

The quartz tube used for soot sampling had an outer diameter of 12 mm, inner diameter of 8 mm, and a tip with a 0.4 mm pinhole (Fig. 1b). The geometry of the tip was developed to minimise flame disturbance and residence time of the sample in the tip before mixing with the diluent. Immediately after the tip, the sample was diluted with approx. 8.5 SLPM N_2 and sucked into a central 6 mm stainless steel tube. By using a similar N_2 dilution flow rates and sample dilution ratios, the volumetric sample flow through the nozzle was kept in a similar range in each experiment. The exact primary dilution ratio was maintained in the range 170–250 by slight adjustments to the N_2 flow rate. The dilution ratio was continuously measured by the DMS500 by setting the diluent flow rate while measuring the amount of gas arriving at the DMS (i.e., diluent plus sample). This ratio was multiplied by the secondary dilution ratio of 500 (see below) and used for the dilution correction. However, the primary dilution ratio was not constant because it

changed depending on the temperature at the probe tip, progressive clogging of the orifice in highly sooting regions of the flame, and limitations of the DMS500 mass flow meters (see below). The diluted sample was passed through a conductive silicon tube (inner diameter 5.4 mm, length 1 m) to a Differential Mobility Spectrometer (Cambustion DMS500), where a further dilution by a factor of 500 was achieved with a rotating disc diluter. The pressure in the sampling line was measured to be close to atmospheric. Given the above parameters, the velocity of the N_2/sample gas in the silicon tube was $\sim$ 6.2 m s^{-1}. This results in a residence time of the sample from the probe to the DMS500 of $\sim$ 0.2 s. It should be noted that sample losses in the lines can be significant for particles <20 nm and sampling lines >1 m [49]. Due to the detection limit of the DMS500 ($\sim$ 5 nm) and the focus of this work on trends for particles >20 nm, DMS500 results were not corrected for diffusional losses. However, the above information and supplemented DMS data set enable the interested reader to do so.

At each HAB, the particle size distribution was recorded for 15 s at a rate of 10 Hz and averaged. Each experiment was repeated four times and error bars are reported as min/max values to indicate the reproducibility of the experiments. A log-normal function was fitted to the measured curves to deconvolute bimodal particle size distributions and to obtain the size and number density of each mode.

2.4. Colour ratio pyrometry

The colour ratio pyrometry experiments were conducted using a Blackfly S camera (BFS-U3-32S4C-C, FLIR Integrated Imaging Solutions, Inc.) having a 1/1.8" Sony IMX252 CMOS sensor with 2048x1536 pixels (pixel size 3.45 μm). The camera lens was a MVL25M23 from Thorlabs with an aperture set to f/1.4 and a focal length of 25 mm. The distance between the camera and the flame was 25 cm, resulting in a pixel width corresponding to 1/34 mm in the focal plane through the centre of the flame. A BG-39 filter (Thorlabs) was used to balance the intensity ratios of the three colour channels and to block infra-red light.

The soot temperature is related to the colour ratio recorded by the camera through [50]:

$$\frac{R_i}{R_j} = \frac{\int_0^\infty \eta_i(\lambda)\frac{1}{\lambda^{5+\alpha}}[\exp(hc/\lambda kT)-1]^{-1}\mathrm{d}\lambda}{\int_0^\infty \eta_j(\lambda)\frac{1}{\lambda^{5+\alpha}}[\exp(hc/\lambda kT)-1]^{-1}\mathrm{d}\lambda}, \tag{2}$$

where R_i is the light intensity of colour channel i, λ is the wavelength, η_i is the wavelength-dependent camera response of colour channel i, and α is

the soot dispersion exponent. The Boltzmann and Planck constants are k and h, respectively, and c is the speed of light. Following the procedure of Ma and Long [51], a hot S-type thermocouple was imaged to calibrate the optical system and to calculate a temperature look-up table relating the camera colour ratio response to the soot temperature. Choosing an α for soot is not trivial as its value changes with soot maturity and thus location in the flame [50]. Accordingly, a range of values for α were reported. Here, a constant value commonly used for colour ratio pyrometry of diffusion flames was used throughout the flame as derived from the wavelength dependant soot absorption function reported in literature [52, 53].

Once the soot temperature is known, the soot volume fraction f_v can be calculated [51, 53, 54]:

$$f_\mathrm{v} = -\frac{\lambda_\mathrm{eff}}{K_\mathrm{ext} L} \ln(1 - \epsilon_\mathrm{L}(\lambda_\mathrm{eff}) \frac{R_\mathrm{i}}{\tau S_\mathrm{L}}). \tag{3}$$

Here, λ_eff is the effective filter wavelength [51], K_ext is the soot dimensionless extinction coefficient (value taken as 8.6 [53]), L is the pixel dimension (1 mm per 34 pixels), and $\epsilon_\mathrm{L}(\lambda_\mathrm{eff})$ is the emissivity at λ_eff of the calibration source (S-type thermocouple). The green colour channel had the highest signal-to-noise ratio and was therefore used for R_i. Images of the hot thermocouple provided the light intensity of the calibration source (S_L). An interpolation of S_L per exposure time as a function of the temperature was used in Eq. 3 at the respective soot temperature calculated previously.

One challenge in colour ratio pyrometry is calculating the required flame cross section intensity R_i from its line of sight projection P_i recorded by the camera. For the reconstruction of R_i, a recently reported Abel inversion methodology was used, called fitting the line-of-sight projection of a predefined intensity distribution (FLiPPID) [55]. Here, a suitable function for the radial intensity distribution in the flame is chosen and its forward Abel transform is fitted to the observed data. A function suitable for co-flow diffusion flames was shown to be [55]:

$$R(r) = \frac{a}{b\sqrt{\pi}} \exp\left[c\left(\frac{r}{b}\right)^2 - \left(\frac{r}{b}\right)^6\right], \tag{4}$$

with a, b, c being fitting parameters. Advantages of this Abel inversion method are that it results in significantly smoother Abel inversion, especially close to the flame centreline, and that nonphysical negative light intensities are avoided. Accordingly, this method was used for the Abel inversion when possible. An exception are images taken while sampling from the flame. FLiPPID would not allow for potential local extrema below the sampling probe.

Therefore, the more commonly applied BASEX Abel inversion [16, 56, 57] was used here. A Python code for obtaining soot temperature and volume fractions with colour ratio pyrometry using different Abel inversion techniques is available online [58].

3. Results and discussion

The fuel, carrier gas, and sheath air flow rates were chosen such that all flames are slightly lifted (1–1.5 mm, Fig. 2) to minimise heat transfer into the fuel tube and to simplify the boundary conditions in any future numerical simulations. The luminescent flame height of the *n*-heptane flame is 37 mm. This apparent flame height is simply based on the region in which soot incandescence can be observed by the naked eye. The stoichiometric flame height is known to be substantially smaller for hydrocarbon flames with high soot concentrations due to an extended soot oxidation zone [59, 60].Adding toluene to the fuel mixture successively increases the visible flame height (41 mm for 15 mol% toluene) and elongates the yellow luminescence zone towards lower height above burner (HAB). A shift of the luminous zone towards lower HAB and elongation of the flame with increasing aromatic content is in agreement with previous reports where *n*-propylbenzene was added to an *n*-dodecane/methane diffusion flame [26]. The given explanation was an earlier soot inception and increased time before complete soot oxidation [26].

The radiation-corrected thermocouple temperatures along the centreline of the four flames are almost identical at low HAB, increasing from 860 K at 3 mm HAB to 1260 K at 17 mm HAB (Fig. 3). At 15 mm HAB, the temperatures start to diverge slightly with the pure heptane flame reaching slightly higher temperatures. At 23 mm HAB, all flames show a local maximum. Above 27 mm HAB, the divergence in flame temperatures becomes more pronounced. All flames reach a local temperature minimum around 27–29 mm HAB after which the temperatures start to increase again.

The temperature difference between the heptane and toluene-containing flames is up to 350 K at 31 mm HAB. Such a dip in the centreline temperature has been observed by numerous researchers. One given explanation was a measuring artefact due to soot deposition on the thermocouple [61, 62]. Even though such an artefact cannot be excluded, the rapid thermocouple injection and extrapolation to time 0 s (i.e., prior to any soot deposition; see Fig. S1) make this explanation unlikely in this case. Another refutation is that similar local minima in the centreline temperature were detected by non-intrusive techniques such as colour ratio pyrometry [17]. An alternative explanation is radiative heat loss from regions with high concentrations of

soot. The importance of radiation and its effect on flame temperature was highlighted by numerous researchers [63, 64]. Even though conclusive proof for the reasons of the dip in centreline temperature is not available, the trends in the temperature profile (Fig. 3) are in line with an increased radiative heat loss in regions with higher soot concentration. The onset where the temperatures of the four flames starts to differ (15 mm HAB) agrees with the location where soot particles start forming (see below). The drop in temperature above 23 mm HAB and local minimum at 27–29 mm HAB coincide with regions of highest soot concentration. Toluene flames, which form more soot (see below), show a more pronounced dip in the temperature profile. The maximum temperature of the heptane flame is at 33 mm HAB (1792 K), while adding toluene reduces the maximum temperature (1716 K for 5 % toluene), potentially due to the increased heat loss. Similarly, the temperature at 39 mm HAB is 120 K lower for the 15% toluene/heptane flame compared to pure heptane.

The transient thermocouple response can give a qualitative impression of the HAB at which soot starts to form (Fig. S3). Note that only the first 10 s are shown in Fig. S3 because this is the region where the steepest temperature decrease would be expected if soot is present due to an increase in the thermocouple emissivity (Fig. S1). For all flames, it took about 1-1.5 s for the thermocouple to approach the flame temperature. For the heptane flame, the temperature remains constant at 11 mm HAB and decreases as a function of time at 13 mm HAB. The decrease in temperature is hereby caused by soot deposition on the thermocouple, causing its emissivity and bead size to increase [38]. The addition of toluene causes a time dependent temperature decrease at lower HAB, indicating earlier soot inception. The earlier soot formation with increasing toluene concentration explains the shift of the luminescence zone towards lower HAB as observed in Fig. 2 and is in agreement with previous reports [22, 23].

The soot temperatures as measured with colour ratio pyrometry are shown in Fig. 4a. Soot temperatures measured by pyrometry and the gas temperature measured with the thermocouple are not directly comparable because of the complex correlation between exothermic reaction in the gas phase and on the particle surface, radiative heat loss from the particles, and uncertainties for both methods (e.g., assumed parameters for radiation correction of thermocouple temperature and assumed α for soot). Nevertheless, similar trends can be observed to the extent that increasing toluene content results in lower centreline temperatures. The estimated soot centreline temperature is observed to decrease by approx. 40 K per 5% of added toluene.

The soot volume fractions of the four studied diffusion flames are shown in Fig. 4b. The figure shows that the addition of toluene results in the

first detection of soot at lower HAB. This trend is even more significant on the flame wings. The maximum soot volume fraction increased gradually from approx. 0.8 ppm for pure *n*-heptane to 2.2 ppm for 15 % toluene in heptane. Soot is detected at larger HAB with increasing toluene content, explaining the observed change in visible flame height (Fig. 2). Note also that the HAB at which the local minimum in the gas temperature was observed (Fig. 3) coincides with the HAB where the highest soot volume fractions were measured (Fig. 4b). This suggests that the decrease in gas temperature might be related to increased radiative heat loss in regions with high soot volume fractions.

It is worth noting that FLiPPID had difficulties to fit the profiles of the toluene-containing flames at some heights above burner. This tendency became more pronounced with increasing toluene content in the fuel mixture. It is believed that the reason is the increase in soot volume fraction and a corresponding increase in light self absorption [50] with increasing toluene content. Soot self absorption would alter the forward Abel transform and spatial light intensity distribution recorded by the camera. This change in distribution would cause a decrease in the quality of the fit obtained using Eq. 4. In terms of absolute soot temperatures and volume fractions, the effect of self absorption was shown to be small for the soot amounts observed here [50]. To assure that the FLiPPID method does not bias the observed trends and absolute values, the same flame images were also analysed with BASEX for the Abel inversion (Fig. S4 in Supporting Information). Identical trends and similar absolute values can be observed but BASEX led to significant noise amplification towards the flame centreline.

Exemplary particle size distributions inside the flame measured with a differential mobility spectrometer (DMS) are shown in Fig. 5 as log-log plots. The full data set can be found in the Supporting Information, Tables S1–S4, as well as in the Apollo University of Cambridge data repository (`https://doi.org/10.17863/CAM.37224`). At 10 mm HAB, an increase in the toluene content leads to more soot particles while at higher HAB, the particle size distribution seems to be shifted towards larger particles. Contour plots with a linear scale for $dN/dlogD_p$ are shown in Fig. 6 as they illustrate the key trends most clearly. The onset of soot formation as determined using the DMS (Fig. 6) indicates that soot starts to form earlier in the flame as the toluene content is increased. This is in good qualitative agreement with the elongated luminescence zone observed in Fig. 2. For all flames, the size and number of soot particles steadily increases with increasing HAB up to about 26 mm HAB. Thus toluene addition does not simply shift the soot production zone towards lower HAB but extends the time for soot formation and growth prior to oxidation. Above 26 mm HAB, the particles continue to increase in size

and the PSD starts to become bimodal (also see Fig. 5c). At increasing HAB, the soot particles continue growing in size with toluene leading to notably larger particles. Most soot is oxidised by 40 mm HAB for the heptane flame but not for the 15 mol% toluene containing flame, explaining the increased flame height with increasing toluene content observed in Fig. 2.

The averaged mean particle size and number densities give a more quantitative insight into the soot evolution inside the four flames (Fig. 7). In case of a bimodal PSD, the two modes are referred to as major (Fig. 7a and b) and minor mode (Fig. 7c and d) based on the number of soot particles they contain. For the heptane flame, the first soot particles can be observed around 15 mm HAB while toluene addition results in earlier soot nucleation (9 mm HAB for 15 mol% toluene). This onset of soot formation agrees well with the HAB at which soot deposition starts to cause the thermocouple temperature to decrease with time (Fig. S3). Intrusive techniques and insufficient sample dilution were reported to shift the apparent point where soot is first observed towards lower HAB [47, 65]. In this work, the DMS500 and the temporal thermocouple measurements first detect soot at the same HAB, implying adequate quenching of the sample. With increasing HAB, the size and number of the soot particles increase steadily up to 25 mm HAB for the heptane flame and 20 mm HAB for the 15 mol% toluene flame (Fig. 7a and b). At 15–21 mm HAB, the particle size distribution shifted towards larger sizes and another mode with average size of 7 nm becomes visible (Fig. 7c and d). It is probable that this minor mode is also present at lower HAB but is obscured by the major mode. The number density of this minor mode decreases with HAB (Fig. 7d), suggesting its consumption by coalescence or aggregation with other particles. Depending on the fuel mixture, the particle number of this minor peak is too small to be detected above 22–26 mm HAB. The reason why the particle size of this minor mode does not change with HAB or fuel composition is currently unclear. Possibly, the probability of these 7 nm particles to collide with the major mode particles is significantly larger. For all HAB and fuel mixtures, the 7 nm particles account for $<1\%$ of the total particle number density. Once they collided with the larger particles, they will disappear from the minor 7 nm mode without changing its average particle size. However, contributions from other factors cannot be excluded, such as diffusional sample losses of small particles in the lines or truncation effects due to the DMS500 detection limit of $\sim$5 nm. Accordingly, the frequently reported inception mode below 5 nm [23, 34, 45] was not observed due to the DMS detection limit.

Following the near linear increase in soot diameter up to 20–25 mm HAB, the particle size increase becomes more rapid (Fig. 7a). Notably, the HAB at which the slope in particle size growth changes (Fig. 7a) coincides approx-

imately with the HAB of maximum particle number density (Fig. 7b). Thus the rapid increase in particle size is accompanied with a decrease in particle number, suggesting that aggregation and agglomeration now dominate. The maximum size varies significantly with fuel structure, increasing from 90 nm for pure heptane to 121 nm for 15 mol% toluene/heptane. Previous DMS500 measurements at the tip of a wick-fed diffusion flame using *n*-heptane/toluene mixtures as fuel showed a similar trend [24]. At 26–30 mm HAB, the PSD starts to become bimodal and a mode with a size around 20 nm becomes visible (Fig. 7c and d). Similar to the minor 7 nm mode between 15–27 mm HAB, the 20 nm mode is expected to be obscured at lower HAB. The size range of about 20 nm [24, 66] is in good agreement with the primary particles frequently observed in TEM [15, 24, 66]. The mean size of these primary particles depends on the fuel structure, increasing from about 19 nm for heptane to 24 nm for 15 mol% toluene-heptane. The trend of increasing primary particle size with increasing toluene content was also observed in TEM images of soot sampled from a wick-fed diffusion flame [24]. The HAB at which the primary particles and soot aggregates/agglomerates reach a maximum size is at 35–36 mm for all fuels. Above 36 mm HAB, both the size and the number of particles decrease, indicating that the soot is rapidly consumed by oxidation. It is worth noting that the DMS500 detected low concentrations of particles above the visible flame tip (Fig. 2) and below the HAB where soot was first detected using pyrometry (Fig. 4b). This is to be expected given that soot below $\sim 1\%$ of the maximum soot volume fraction will not be detected with this colour ratio pyrometry technique. The reason is that the flame images were taken such that none of the colour channels was saturated at the brightest region in the flame (i.e., the largest amount of soot). In case of the particles above the visible flame tip, a further reason is that the method used to sample the particles has been shown to draw in aerosol from 1-2 mm below the orifice [65]. The combination of actively drawing in soot samples, the limited sensitivity of the camera, and the fact that the visible flame height is not an exact measure all contribute to why visible flame height and height where the DMS500 stopped detecting particles do not match exactly. None of the flames were smoking on the basis that, aside from the issues discussed above, no particles were detected by the DMS500 at larger HAB.

The maximum number density is similar for all flames (Fig. 7b). It should be noted that the similarity between the four studied flames in terms of maximum number density is not caused by limitations of the DMS500. This can be seen when decreasing the ary dilution during sampling (Fig. S7). As expected, the number of detected particles increases with decreasing secondary dilution. In fact, the DMS can resolve number densities at least 600x greater

than the maximum number density reported for any of the other experiments. The key difference between the four fuel mixtures is the HAB at which soot nucleation starts. Soot formed earlier in the flame has more time to grow in size prior to oxidation, explaining the larger primary particle size as seen in Fig. 7c. The larger primaries collide to form larger aggregates and agglomerates as seen in 7a. The morphology of these agglomerates/aggregates was not studied here, thus the relationship between soot size and volume fraction or mass is unknown. Assuming spherical particles is an oversimplification but can nevertheless give a rough estimate of the order of magnitude in soot volume change. Keeping the soot number constant but increasing its size from 91 nm (heptane) to 121 nm (15 mol% toluene-heptane) would increase the soot volume by a factor of 2.4. This significant increase in soot volume fraction would cause higher heat loss from the flame due to thermal radiation, which can be observed in Fig. 3. It is also interesting to note that this factor (2.4) is quite similar to the increase in soot volume fraction observed by colour ratio pyrometry (approx. 2.75). Therefore, an increase in soot particle size is sufficient to explain the increase in soot volume fraction and a significant increases in the soot number density is not required.

It is worth noting that the uncertainties in the dilution corrected soot numbers are not caused by changes in the experimental conditions. Notably, the measured particle size distributions remain stable with time (Fig. S5a). The dilution factor recorded by the DMS fluctuated significantly however due to the limitations of the mass flow meters inside the DMS, introducing significant fluctuations into the dilution corrected number densities (Fig. S5b). This explains the relatively small error bars in the mean particle sizes (Fig. 7a and c) but large uncertainties in the number densities (Fig. 7b and d). Therefore, a more accurate method to measure sample dilutions is expected to have the most significant impact on decreasing the experimental uncertainties.

To assess the flame perturbation during the intrusive aerosol sampling, colour ratio pyrometry experiments were conducted while sampling from within the flame (Fig. 8). BASEX was used for the inverse Abel transform to assure that potential local extrema below the probe orifice are detected. A potential risk in applying colour ratio pyrometry while sampling is that the symmetry of the cylindrical flame, as is assumed for the Abel inversion, is impaired even below the probe orifice. However, the effect of the probe on the flame symmetry below the sampling point was found to be small, as can be seen in the raw images (Fig. S6 in Supporting Information). It might be worthwhile to image the flame from different angles while sampling from the flame to confirm that the symmetry below the orifice is not impaired. However, this was not possible with the current setup and performing the inverse Abel transform is obligatory for obtaining soot temperatures and

volume fractions. As can be seen in Fig. 8, neither the soot temperature nor soot volume fraction profiles are altered significantly below the quartz probe. Most importantly, Fig. 8 shows that the quartz probe used here does not cause temperature drops by up to 500–700 K and flame disturbance by more than 3 mm below the sampling point, as reported for hole-in-tube probes [45, 46]. One reason for the significant temperature drops below the hole-in-tube probes is that several L min^{-1} of cold nitrogen are commonly used for sample quenching and dilution. Thus the tube probe inside the flame is constantly cooled in this configuration. For the quartz probe used here, the diluent nitrogen does not cool the tip where the sample is taken. Other advantages of the quartz probe are its smaller size, causing less pertubations to the flow field below the sampling point. Of course, the flame geometry and symmetry is altered above the sampling point (Fig. S6 in Supporting Information) but this has no effect on the time-temperature history of the sampled particles.

4. Conclusions

A well-established Yale burner was extended by a vapour delivery system to study soot formation during the combustion of more realistic, liquid hydrocarbons. The effect of toluene on the soot particle evolution inside an *n*-heptane flame was characterised by measuring the particle size distribution with a differential mobility spectrometer. The soot samples from the flame centreline were hereby taken with a newly developed quartz probe that is expected to cause less flame disturbance and enhance diluent/sample mixing. Colour ratio pyrometry experiments were used to show that there were no major disturbances in the soot temperature or volume fraction below the probe. The DMS results showed that soot inception starts closer to the burner when the proportion of toluene is increased. This finding is in agreement with the luminescence zone observed in flame photographs. This change in soot nucleation onset was in agreement with the HAB at which soot starts to deposit on the thermocouple, causing the measured temperature to decrease with time. The earlier soot inception is suggested to be caused by much higher rates of PAH formation in the presence of toluene. The earlier soot inception in the toluene-containing flames increased the time for soot growth prior to oxidation. The resulting larger particles inside the toluene flames agrees with the increase in soot volume fraction observed with the pyrometry experiments. These larger amounts of soot required more time to fully oxidise, which explains the increase in the luminescent flame height. The experimental particle size distribution measurements inside a vapour-fed co-flow diffusion flame are the first of their kind and can aid the soot

simulation community in testing their models.

Acknowledgements

This project is funded by the National Research Foundation (NRF), Prime Minister's Office, Singapore under its Campus for Research Excellence and Technological Enterprise (CREATE) programme.

References

[1] J. Lelieveld, J. S. Evans, M. Fnais, D. Giannadaki, A. Pozzer, The contribution of outdoor air pollution sources to premature mortality on a global scale, Nature 525 (2015) 367–371. doi:10.1038/nature15371.

[2] Ö. Gustafsson, V. Ramanathan, Convergence on climate warming by black carbon aerosols, Proc. Natl. Acad. Sci. U.S.A. 113 (2016) 4243–4245. doi:10.1073/pnas.1603570113.

[3] V. Ramanathan, G. Carmichael, Global and regional climate changes due to black carbon, Nat. Geosci. 1 (2008) 221–227. doi:10.1038/ngeo156.

[4] M. Z. Jacobson, Control of fossil-fuel particulate black carbon and organic matter, possibly the most effective method of slowing global warming, J. Geophys. Res.: Atmos. 107 (2002) 4410. doi:10.1029/2001JD001376.

[5] A. Payne, R. Whittaker, Reinforcement of rubber with carbon black, Compos. 1 (1970) 203–214. doi:10.1016/0010-4361(70)90005-4.

[6] J.-C. Huang, Carbon black filled conducting polymers and polymer blends, Adv. Polym. Technol. 21 (2002) 299–313. doi:10.1002/adv.10025.

[7] R. Alcántara, J. M. Jiménez-Mateos, P. Lavela, J. L. Tirado, Carbon black: a promising electrode material for sodium-ion batteries, Electrochem. Commun. 3 (2001) 639–642. doi:10.1016/S1388-2481(01)00244-2.

[8] K.-S. Yun, B.-R. Kim, E. Noh, H.-J. Jung, H.-J. Oh, W.-S. Kang, S.-C. Jung, S.-T. Myung, S.-J. Kim, Microstructural Effect of Carbon Blacks for the Application in Lithium Ion Batteries, Jpn. J. Appl. Phys. 52 (2013) 11NM01. doi:10.7567/JJAP.52.11NM01.

[9] C. S. McEnally, L. D. Pfefferle, B. Atakan, K. Kohse-Höinghaus, Studies of aromatic hydrocarbon formation mechanisms in flames: Progress towards closing the fuel gap, Prog. Energy Combust. Sci. 32 (2006) 247–294. doi:10.1016/j.pecs.2005.11.003.

[10] F. N. Egolfopoulos, N. Hansen, Y. Ju, K. Kohse-Höinghaus, C. K. Law, F. Qi, Advances and challenges in laminar flame experiments and implications for combustion chemistry, Prog. Energy Combust. Sci. 43 (2014) 36–67. doi:10.1016/j.pecs.2014.04.004.

[11] Y. R. Tan, M. L. Botero, Y. Sheng, J. A. H. Dreyer, R. Xu, W. Yang, M. Kraft, Sooting characteristics of polyoxymethylene dimethyl ether blends with diesel in a diffusion flame, Fuel 224 (2018) 499–506. doi:10.1016/j.fuel.2018.03.051.

[12] C. McEnally, A. Schaffer, M. Long, L. Pfefferle, M. Smooke, M. Colket, R. Hall, Computational and experimental study of soot formation in a coflow, laminar ethylene diffusion flame, Proc. Combust. Inst. 27 (1998) 1497–1505. doi:10.1016/S0082-0784(98)80557-2.

[13] M. Smooke, M. Long, B. Connelly, M. Colket, R. Hall, Soot formation in laminar diffusion flames, Combust. Flame 143 (2005) 613–628. doi:10.1016/J.COMBUSTFLAME.2005.08.028.

[14] N. J. Kempema, M. B. Long, Combined optical and TEM investigations for a detailed characterization of soot aggregate properties in a laminar coflow diffusion flame, Combust. Flame 164 (2016) 373–385. doi:10.1016/J.COMBUSTFLAME.2015.12.001.

[15] M. L. Botero, N. Eaves, J. A. Dreyer, Y. Sheng, J. Akroyd, W. Yang, M. Kraft, Experimental and numerical study of the evolution of soot primary particles in a diffusion flame, Proc. Combust. Inst. (2018). doi:10.1016/J.PROCI.2018.06.185.

[16] D. D. Das, P. C. St. John, C. S. McEnally, S. Kim, L. D. Pfefferle, Measuring and predicting sooting tendencies of oxygenates, alkanes, alkenes, cycloalkanes, and aromatics on a unified scale, Combust. Flame 190 (2018) 349–364. doi:10.1016/J.COMBUSTFLAME.2017.12.005.

[17] D. D. Das, W. J. Cannella, C. S. McEnally, C. J. Mueller, L. D. Pfefferle, Two-dimensional soot volume fraction measurements in flames doped with large hydrocarbons, Proc. Combust. Inst. 36 (2017) 871–879. doi:10.1016/j.proci.2016.06.047.

[18] C. S. McEnally, L. D. Pfefferle, Sooting tendencies of nonvolatile aromatic hydrocarbons, Proc. Combust. Inst. 32 (2009) 673–679. doi:10.1016/J.PROCI.2008.06.197.

[19] C. S. McEnally, L. D. Pfefferle, Sooting Tendencies of Oxygenated Hydrocarbons in Laboratory-Scale Flames, Environ. Sci. Technol. 45 (2011) 2498–2503. doi:10.1021/es103733q.

[20] C. S. McEnally, L. D. Pfefferle, Improved sooting tendency measurements for aromatic hydrocarbons and their implications for naphthalene formation pathways, Combust. Flame 148 (2007) 210–222. doi:10.1016/J.COMBUSTFLAME.2006.11.003.

[21] D. D. Das, C. S. McEnally, T. A. Kwan, J. B. Zimmerman, W. J. Cannella, C. J. Mueller, L. D. Pfefferle, Sooting tendencies of diesel fuels, jet fuels, and their surrogates in diffusion flames, Fuel 197 (2017) 445–458. doi:10.1016/j.fuel.2017.01.099.

[22] C. S. McEnally, L. D. Pfefferle, Experimental Assessment of Naphthalene Formation Mechanisms in Non-Premixed Flames, Combust. Sci. Technol. 128 (1997) 257–278. doi:10.1080/00102209708935712.

[23] Q. Tang, B. Ge, Q. Ni, B. Nie, X. You, Soot formation characteristics of n-heptane/toluene mixtures in laminar premixed burner-stabilized stagnation flames, Combust. Flame 187 (2018) 239–246. doi:10.1016/j.combustflame.2017.08.022.

[24] M. L. Botero, S. Mosbach, M. Kraft, Sooting tendency and particle size distributions of n-heptane/toluene mixtures burned in a wick-fed diffusion flame, Fuel 169 (2016) 111–119. doi:10.1016/j.fuel.2015.12.014.

[25] A. E. Daca, Ö. L. Gülder, Soot formation characteristics of diffusion flames of methane doped with toluene and n -heptane at elevated pressures, Proc. Combust. Inst. 36 (2017) 737–744. doi:10.1016/j.proci.2016.07.046.

[26] T. Zhang, L. Zhao, M. J. Thomson, Effects of n-propylbenzene addition to n-dodecane on soot formation and aggregate structure in a laminar coflow diffusion flame, Proc. Combust. Inst. 36 (2017) 1339–1347. doi:10.1016/j.proci.2016.05.026.

[27] H. Calcote, D. Manos, Effect of molecular structure on incipient soot formation, Combust. Flame 49 (1983) 289–304. doi:10.1016/0010-2180(83)90172-4.

[28] E. J. Barrientos, M. Lapuerta, A. L. Boehman, Group additivity in soot formation for the example of C-5 oxygenated hydrocarbon fuels, Combust. Flame 160 (2013) 1484–1498. doi:10.1016/J.COMBUSTFLAME.2013.02.024.

[29] M. L. Botero, S. Mosbach, J. Akroyd, M. Kraft, Sooting tendency of surrogates for the aromatic fractions of diesel and gasoline in a wick-fed diffusion flame, Fuel 153 (2015) 31–39. doi:10.1016/j.fuel.2015.02.108.

[30] A. D. Abid, J. Camacho, D. A. Sheen, H. Wang, Quantitative measurement of soot particle size distribution in premixed flames – The burner-stabilized stagnation flame approach, Combust. Flame 156 (2009) 1862–1870. doi:10.1016/j.combustflame.2009.05.010.

[31] 4th International Sooting Flame (ISF) Workshop.
URL https://www.adelaide.edu.au/cet/isfworkshop/2018-workshop/

[32] A. Naseri, A. Veshkini, M. J. Thomson, Detailed modeling of CO_2 addition effects on the evolution of soot particle size distribution functions in premixed laminar ethylene flames, Combust. Flame 183 (2017) 75–87. doi:10.1016/j.combustflame.2017.04.028.

[33] R. P. Lindstedt, B. B. O. Waldheim, Modeling of soot particle size distributions in premixed stagnation flow flames, Proc. Combust. Inst. 34 (2013) 1861–1868. doi:10.1016/j.proci.2012.05.047.

[34] E. K. Yapp, D. Chen, J. Akroyd, S. Mosbach, M. Kraft, J. Camacho, H. Wang, Numerical simulation and parametric sensitivity study of particle size distributions in a burner-stabilised stagnation flame, Combust. Flame 162 (2015) 2569–2581. doi:10.1016/j.combustflame.2015.03.006.

[35] A. Khosousi, F. Liu, S. B. Dworkin, N. A. Eaves, M. J. Thomson, X. He, Y. Dai, Y. Gao, F. Liu, S. Shuai, J. Wang, Experimental and numerical study of soot formation in laminar coflow diffusion flames of gasoline/ethanol blends, Combust. Flame 162 (2015) 3925–3933. doi:10.1016/j.combustflame.2015.07.029.

[36] A. Veshkini, N. A. Eaves, S. B. Dworkin, M. J. Thomson, Application of PAH-condensation reversibility in modeling soot growth in laminar premixed and nonpremixed flames, Combust. Flame 167 (2016) 335–352. doi:10.1016/j.combustflame.2016.02.024.

[37] E. K. Y. Yapp, R. I. A. Patterson, J. Akroyd, S. Mosbach, E. M. Adkins, J. Houston Miller, M. Kraft, Numerical simulation and parametric sensitivity study of optical band gap in a laminar co-flow ethylene diffusion flame, Combust. Flame 167 (2016) 320–334. doi:10.1016/j.combustflame.2016.01.033.

[38] G. De Falco, M. Commodo, A. D'Anna, P. Minutolo, The evolution of soot particles in premixed and diffusion flames by thermophoretic particle densitometry, Proc. Combust. Inst. 36 (2017) 763–770. doi:10.1016/j.proci.2016.07.108.

[39] C. S. McEnally, Ü. Ö. Köylü, L. D. Pfefferle, D. E. Rosner, Soot volume fraction and temperature measurements in laminar nonpremixed flames using thermocouples, Combust. Flame 109 (1997) 701–720. doi:10.1016/S0010-2180(97)00054-0.

[40] C. R. Shaddix, Correcting thermocouple measurements for radiation loss: A critical review, in: Proceedings of the 33rd National Heat Transfer Conference, Albuquerque, New Mexico, American Society of Mechanical Engineers, Albuquerque, NM, USA, 1999, pp. HTD99–282.

[41] V. Gnielinski, VDI-Wärmeatlas, Springer-Verlag Berlin Heidelberg, 2013, p. 817.

[42] M. Conturso, M. Sirignano, A. D'Anna, Effect of 2,5-dimethylfuran doping on particle size distributions measured in premixed ethylene/air flames, Proc. Combust. Inst. 36 (2017) 985–992. doi:10.1016/j.proci.2016.06.048.

[43] M. Kazemimanesh, A. Moallemi, J. S. Olfert, L. W. Kostiuk, Probe sampling to map and characterize nanoparticles along the axis of a laminar methane jet diffusion flame, Proc. Combust. Inst. 36 (2017) 881–888. doi:10.1016/j.proci.2016.06.169.

[44] M. Commodo, A. D'Anna, G. De Falco, R. Larciprete, P. Minutolo, Illuminating the earliest stages of the soot formation by photoemission and Raman spectroscopy, Combust. Flame 181 (2017) 188–197. doi:10.1016/j.combustflame.2017.03.020.

[45] B. Zhao, Z. Yang, J. Wang, M. V. Johnston, H. Wang, Analysis of Soot Nanoparticles in a Laminar Premixed Ethylene Flame by Scanning Mobility Particle Sizer, Aerosol Sci. Technol. 37 (2003) 611–620. doi:10.1080/02786820300908.

[46] M. Commodo, G. De Falco, A. Bruno, C. Borriello, P. Minutolo, A. D'Anna, Physicochemical evolution of nascent soot particles in a laminar premixed flame: from nucleation to early growth, Combust. Flame 162 (2015) 3854–3863. doi:10.1016/j.combustflame.2015.07.022.

[47] H. Hepp, K. Siegmann, Mapping of soot particles in a weakly sooting diffusion flame by aerosol techniques, Combust. Flame 115 (1998) 275–283. doi:10.1016/S0010-2180(97)00346-5.

[48] E. Goudeli, A. J. Gröhn, S. E. Pratsinis, Sampling and dilution of nanoparticles at high temperature, Aerosol Sci. Technol. 50 (2016) 591–604. doi:10.1080/02786826.2016.1168922.

[49] P. Kumar, P. Fennell, J. Symonds, R. Britter, Treatment of losses of ultrafine aerosol particles in long sampling tubes during ambient measurements, Atmos. Environ. 42 (38) (2008) 8819–8826. doi:10.1016/J.ATMOSENV.2008.09.003.

[50] N. J. Kempema, M. B. Long, Effect of soot self-absorption on color-ratio pyrometry in laminar coflow diffusion flames, Opt. Lett. 43 (2018) 1103–1106. doi:10.1364/OL.43.001103.

[51] B. Ma, M. B. Long, Absolute light calibration using S-type thermocouples, Proc. Combust. Inst. 34 (2) (2013) 3531–3539. doi:10.1016/j.proci.2012.05.030.

[52] H. Chang, T. T. Charalampopoulos, Determination of the Wavelength Dependence of Refractive Indices of Flame Soot, Proc. R. Soc. A 430 (1990) 577–591. doi:10.1098/rspa.1990.0107.

[53] P. B. Kuhn, B. Ma, B. C. Connelly, M. D. Smooke, M. B. Long, Soot and thin-filament pyrometry using a color digital camera, Proc. Combust. Inst. 33 (2011) 743–750. doi:10.1016/j.proci.2010.05.006.

[54] F. Cignoli, S. De Iuliis, V. Manta, G. Zizak, Two-dimensional two-wavelength emission technique for soot diagnostics, Appl. Opt. 40 (2001) 5370–5378. doi:10.1364/AO.40.005370.

[55] J. A. H. Dreyer, R. I. Slavchov, E. J. Rees, J. Akroyd, M. Salamanca, S. Mosbach, M. Kraft, Improved methodology for performing the inverse abel transform of flame images for colour ratio pyrometry, Appl. Opt. 58 (2019) 2662–2670. doi:10.1364/AO.58.002662.

[56] M. Apostolopoulos, M. Taroudakis, D. Papazoglou, Application of inverse Abel techniques in in-line holographic microscopy, Opt. Commun. 296 (2013) 25–34. doi:10.1016/J.OPTCOM.2013.01.053.

[57] V. Dribinski, A. Ossadtchi, V. A. Mandelshtam, H. Reisler, Reconstruction of Abel-transformable images: The Gaussian basis-set expansion Abel transform method, Rev. Sci. Instrum. 73 (2002) 2634–2642. doi:10.1063/1.1482156.

[58] J. A. H. Dreyer, R. I. Slavchov, A. Menon, "Flame pyrometry" (CoMo website, 2019), https://como.cheng.cam.ac.uk/index.php?Page=FlamePyrometry.

[59] A. S. Gordon, S. C. Li, F. A. Williams, Visible flame heights of laminar coflow diffusion flames, Combust. Sci. Technol. 141 (1) (1999) 1–18. doi:10.1080/00102209908924179.

[60] F. G. Roper, C. Smith, A. C. Cunningham, The prediction of laminar jet diffusion flame sizes: Part II. Experimental verification, Combust. Flame 29 (1977) 227–234. doi:10.1016/0010-2180(77)90113-4.

[61] K. Hayashida, T. Mogi, K. Amagai, M. Arai, Growth characteristics of polycyclic aromatic hydrocarbons in dimethyl ether diffusion flame, Fuel 90 (2011) 493–498. doi:10.1016/J.FUEL.2010.10.012.

[62] K. Hayashida, S. Nagaoka, H. Ishitani, Growth and oxidation of graphitic crystallites in soot particles within a laminar diffusion flame, Fuel 128 (2014) 148–154. doi:10.1016/J.FUEL.2014.03.008.

[63] M. Saffaripour, A. Veshkini, M. Kholghy, M. J. Thomson, Experimental investigation and detailed modeling of soot aggregate formation and size distribution in laminar coflow diffusion flames of Jet A-1, a synthetic kerosene, and n-decane, Combust. Flame 161 (2014) 848–863. doi:10.1016/J.COMBUSTFLAME.2013.10.016.

[64] M. D. Smooke, R. J. Hall, M. B. Colket 4, J. Fielding, M. B. Long, C. S. McEnally, L. D. Pfefferle, Investigation of the transition from lightly

sooting towards heavily sooting co-flow ethylene diffusion flames, Combust. Theory Modell. 8 (3) (2004) 593–606. doi:10.1088/1364-7830/8/3/009.

[65] C. Saggese, A. Cuoci, A. Frassoldati, S. Ferrario, J. Camacho, H. Wang, T. Faravelli, Probe effects in soot sampling from a burner-stabilized stagnation flame, Combust. Flame 167 (2016) 184–197. doi:10.1016/j.combustflame.2016.02.013.

[66] Z. Li, L. Qiu, X. Cheng, Y. Li, H. Wu, The evolution of soot morphology and nanostructure in laminar diffusion flame of surrogate fuels for diesel, Fuel 211 (2018) 517–528. doi:10.1016/j.fuel.2017.09.036.

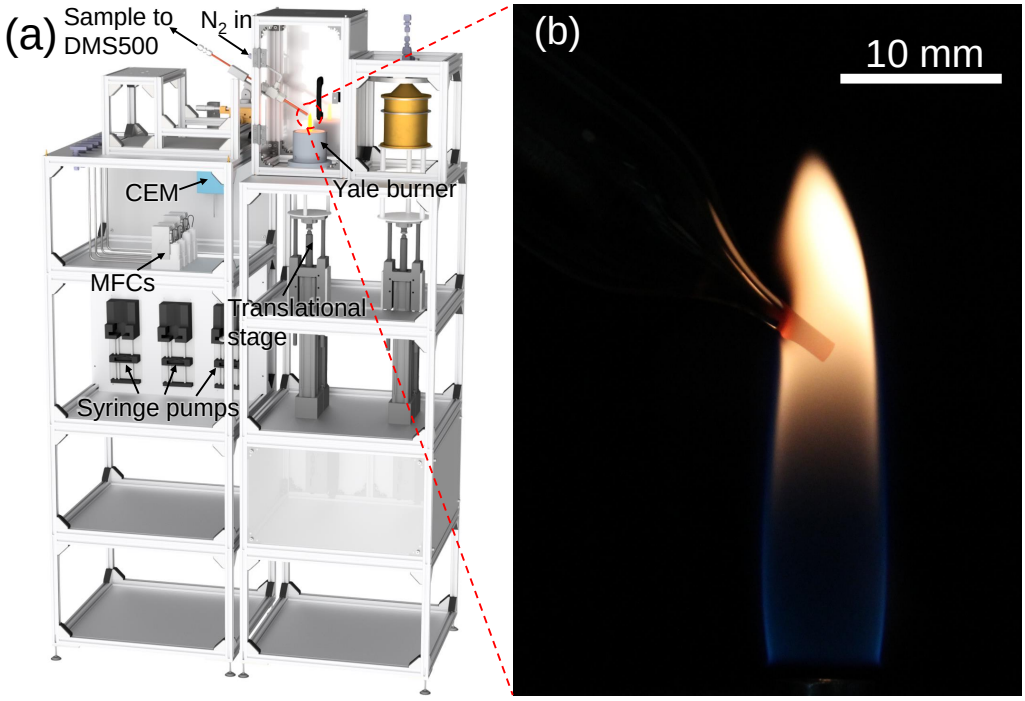

Figure 1: (a) Experimental flame set-up for the vapour-fed co-flow diffusion flame. (b) Soot sampling using a quartz tube with a 0.4 mm orifice.

Figure 2: Photographs of the co-flow diffusion flames fed with four different fuel compositions but identical fuel mass flow rates. From left to right: pure n-heptane, 5 mol% toluene/heptane, 10 mol% toluene/heptane, 15 mol% toluene/heptane. Identical camera settings were used for all images.

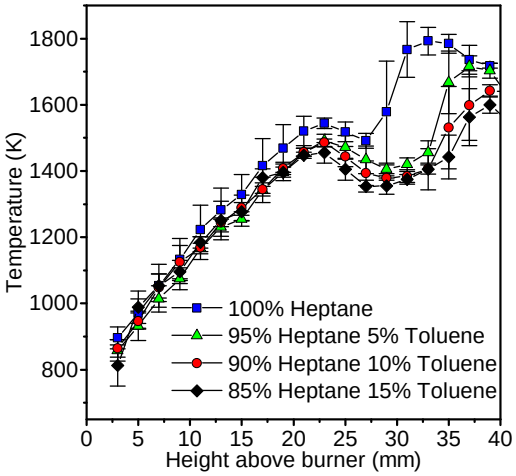

Figure 3: Radiation-corrected thermocouple temperatures measured along the centreline as a function of HAB and fuel composition. The error bars show the 95% confidence interval. The averaged temperature was generally within 100 K of the max/min measured values but larger uncertainties were observed where high spatial temperature gradients were present (e.g., 29 mm HAB for the 100% heptane flame).

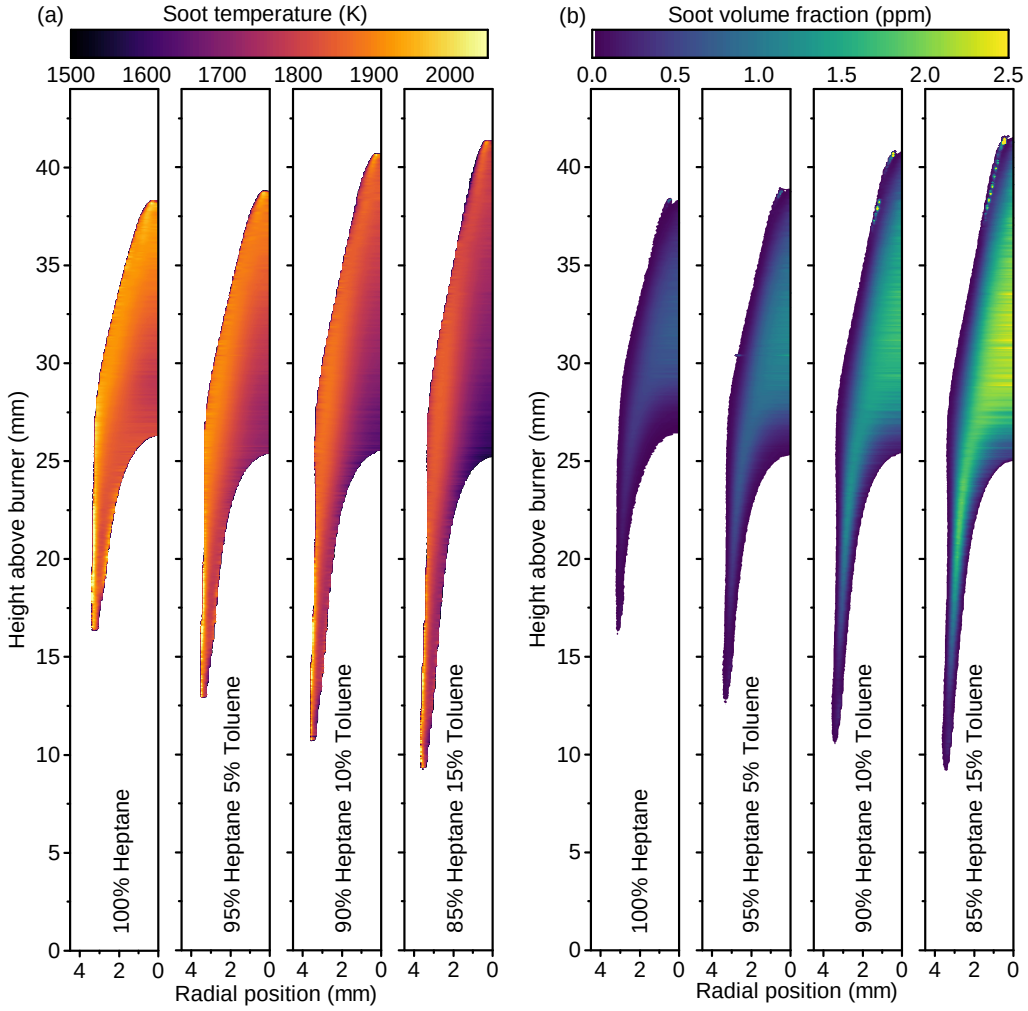

Figure 4: (a) Soot temperatures and (b) volume fractions of the four studied diffusion flames measured with colour-ratio pyrometry.

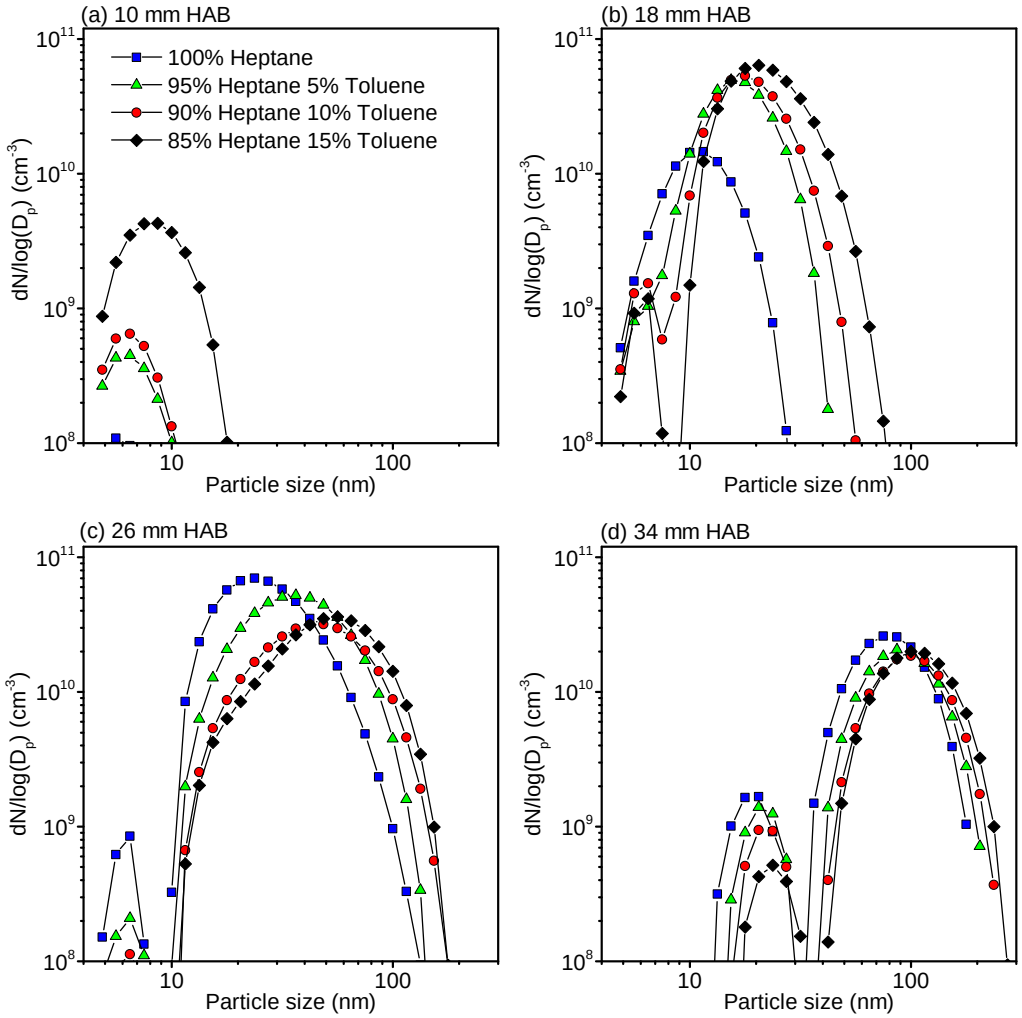

Figure 5: Particle size distributions inside the four studied diffusion flames at (a) 10 mm HAB, (b) 18 mm HAB, (c) 26 mm HAB, and (d) 34 mm HAB. The averaged values from four measurements are shown. For clarity, the uncertainty bounds are not shown in this particular figure.

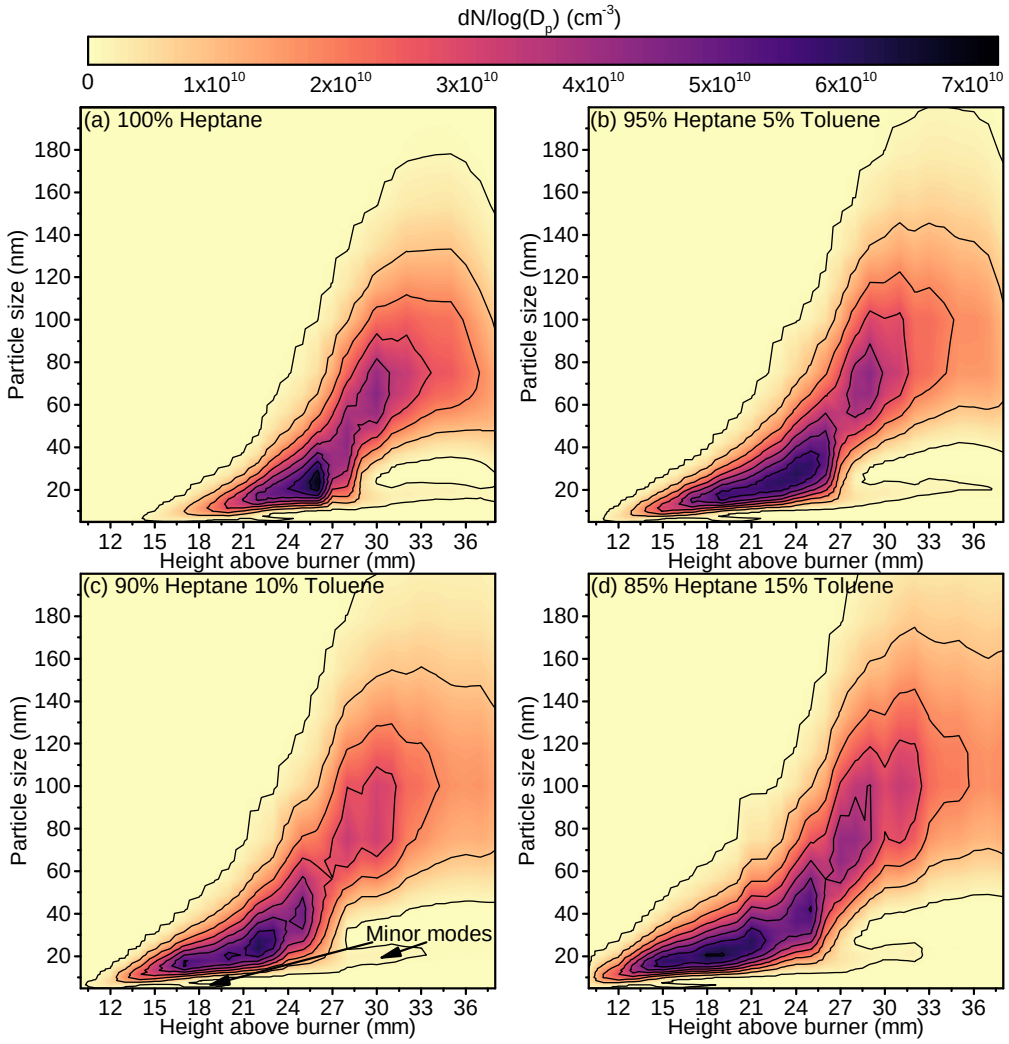

Figure 6: Measured centreline particle size distribution as function of height above burner and fuel structure. The minor mode discussed in the text and quantified in Fig. 7 is indicated in (c).

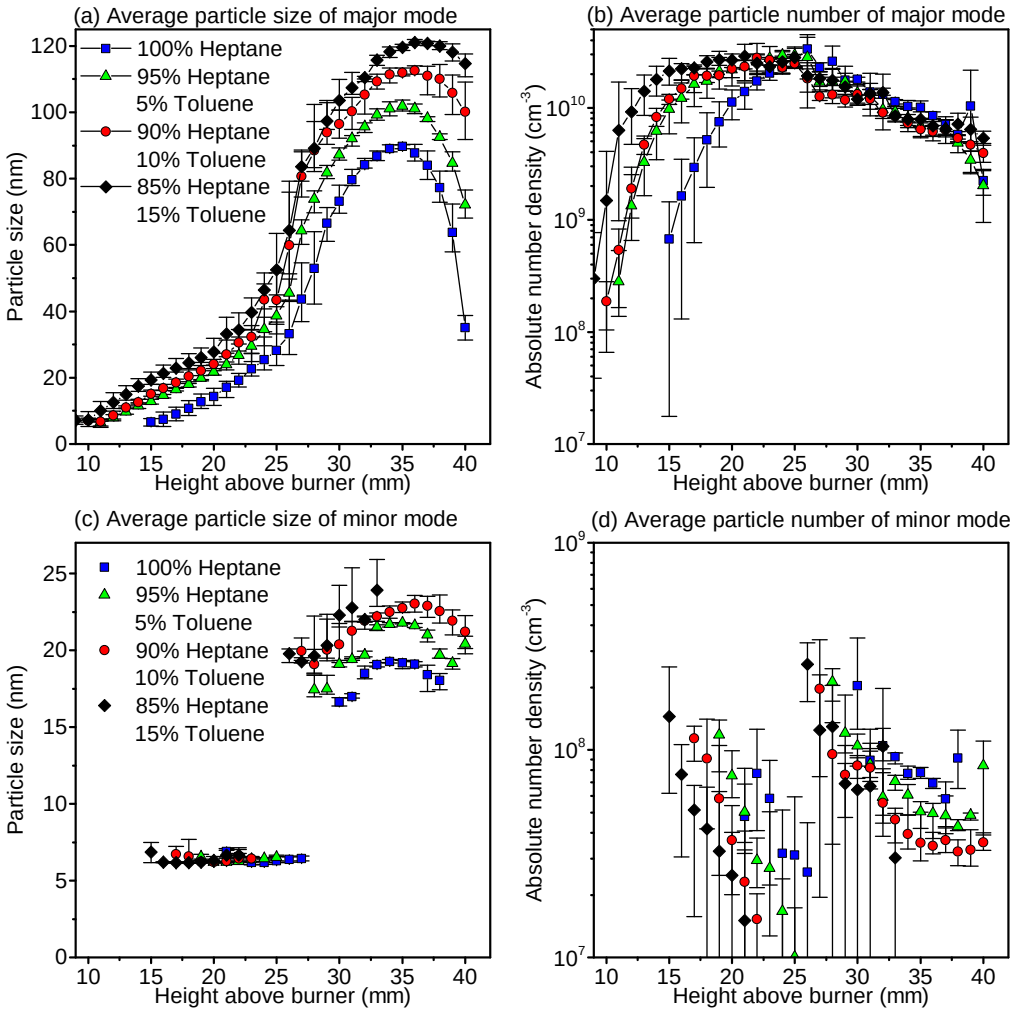

Figure 7: Particle sizes and number densities of the major and minor modes observed in the particle size distribution. The error bars represent the max. and min. values.

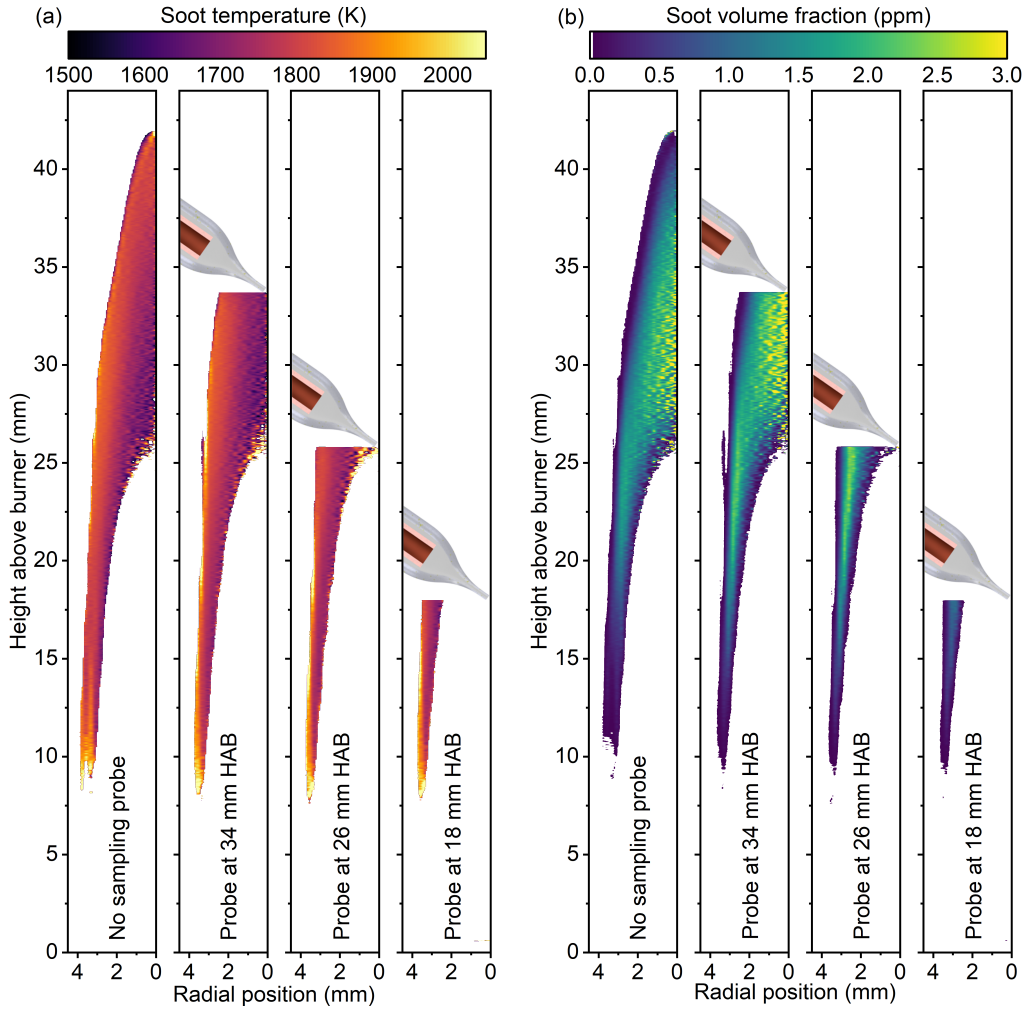

Figure 8: (a) Soot temperatures and (b) volume fractions of the 85% Heptane 15% Toluene flame while sampling. The sampling probe position is shown schematically.

Supplementary material: Evolution of the soot particle size distribution along the centreline of an *n*-heptane/toluene co-flow diffusion flame

Jochen A.H. Dreyer[a,b,e], Maximilian Poli[a], Nick Eaves[a], Maria L. Botero[c], Jethro Akroyd[a,e], Sebastian Mosbach[a,e], Markus Kraft[a,d,e,*]

[a] *Department of Chemical Engineering and Biotechnology, University of Cambridge, Philippa Fawcett Drive, Cambridge, CB3 0AS, United Kingdom*
[b] *CoaST, Department of Chemical and Biochemical Engineering, Technical University of Denmark (DTU), Building 229, 2800, Kgs. Lyngby, Denmark*
[c] *Department of Mechanical Engineering, National University of Singapore, 9 Engineering Drive, 117576 Singapore*
[d] *School of Chemical, and Biomedical Engineering, Nanyang Technological University, 62 Nanyang Drive, 637459 Singapore*
[e] *Cambridge Centre for Advanced Research and Education in Singapore (CARES), CREATE Tower, 1 Create Way, 138602 Singapore*

Supporting information

These supporting information provide additional figures and tables to substantiate the results and discussions presented in the main article. In addition, all the raw data presented in Fig. 6 of the main manuscript are provided in Tables S1–S4 to facilitate the validation of numerical soot models and comparison to other experimental studies. Note that the data is also available in csv format in the Apollo University of Cambridge data repository (`https://doi.org/10.17863/CAM.37224`). The values are corrected for dilution and the temperature at the sampling probe tip but not sample losses in the lines. The numbers are in $\mathrm{dN/dlogD_p}$ ($\mathrm{cm^{-3}}$); the absolute particle number density can be obtained by summation over all particle sizes and dividing by 16 in accordance with the DMS500 manual. A technical drawing of the quartz probe developed to take the soot samples from within the flame is shown on the last page.

*E-mail: mk306@cam.ac.uk

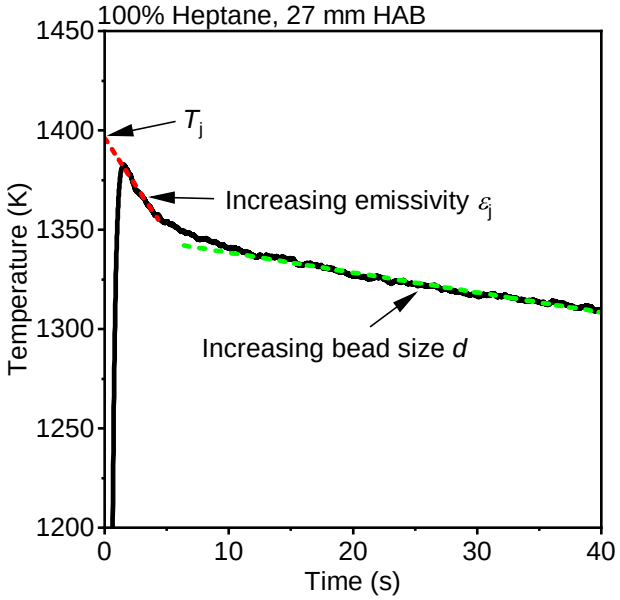

Figure S1: Example of the measured thermocouple temperature as function of time in regions with high soot concentrations. A linear extrapolation of the first slope (increasing emissivity) to time 0 s was used to estimate the junction temperature, T_j.

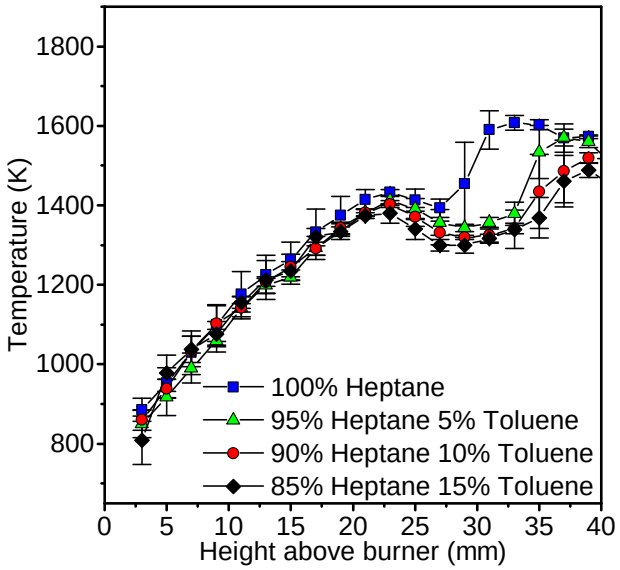

Figure S2: Uncorrected flame temperatures as measured by fast insertion of a S-type thermocouple.

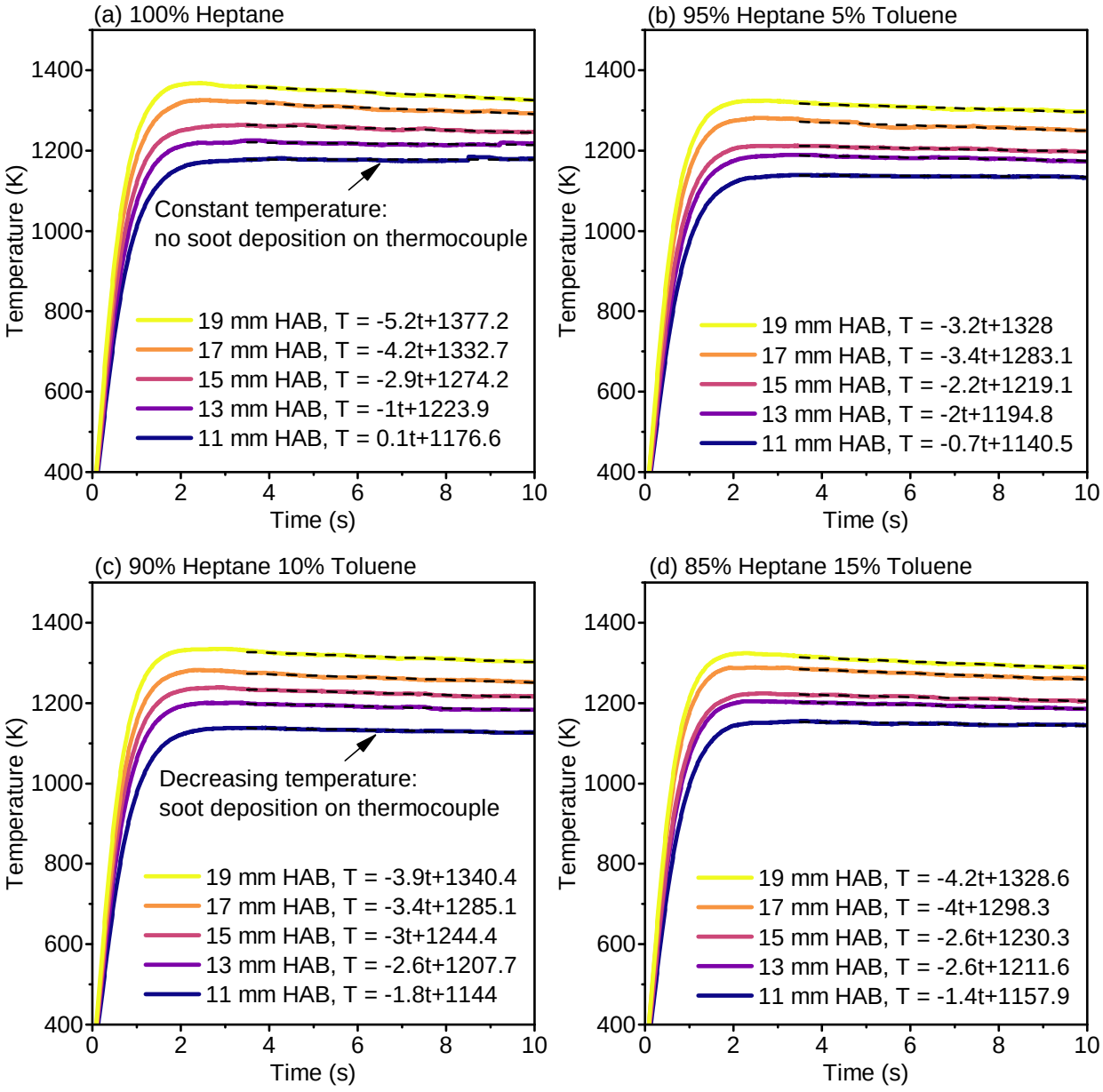

Figure S3: Time resolved flame temperature measurements at different HAB. The dashed lines are linear regressions between 3.5-10 s and the resulting equations are shown in the figure legends.

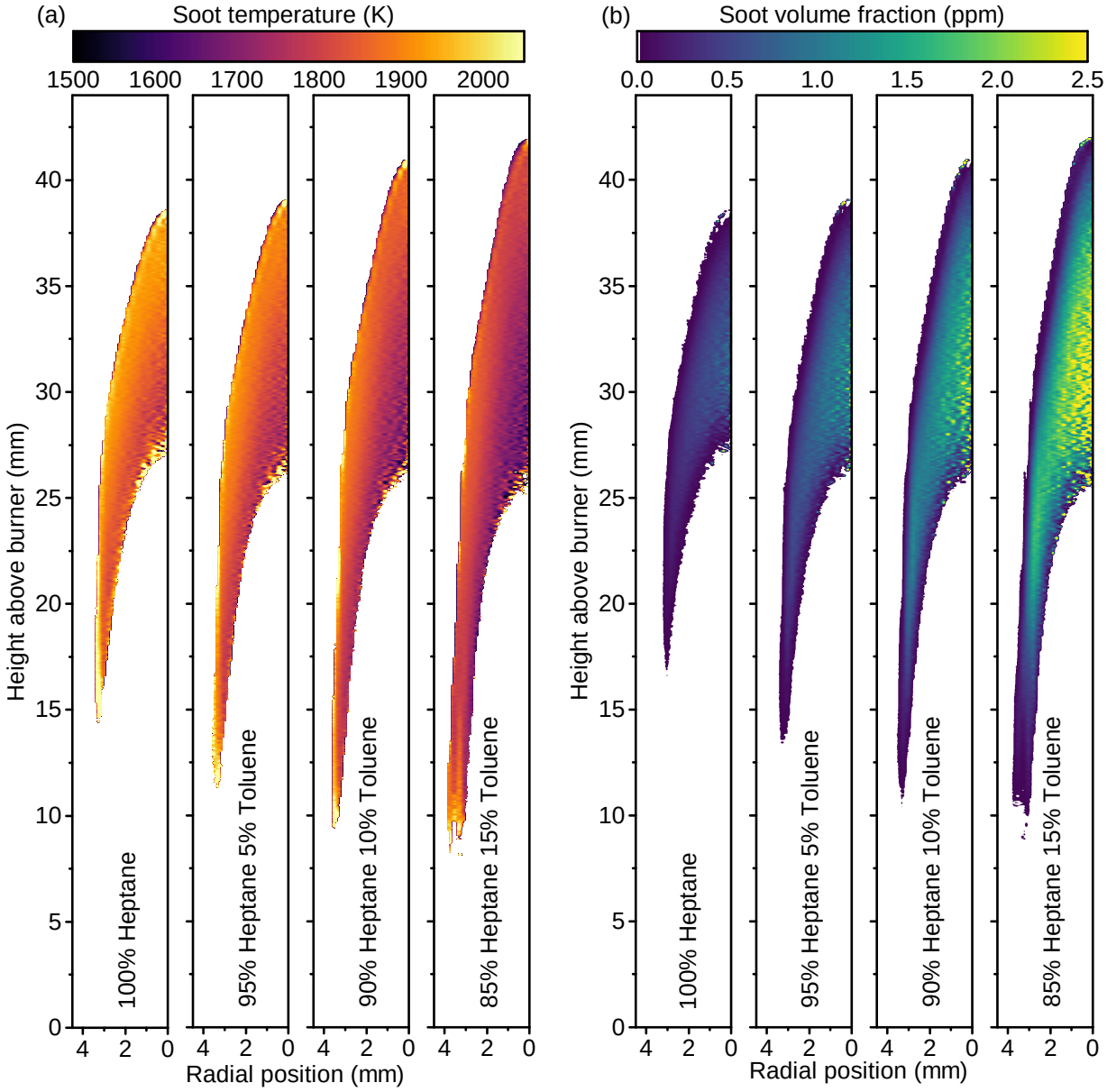

Figure S4: (a) Soot temperature and (b) volume fraction obtained using BASEX for the inverse Abel transform.

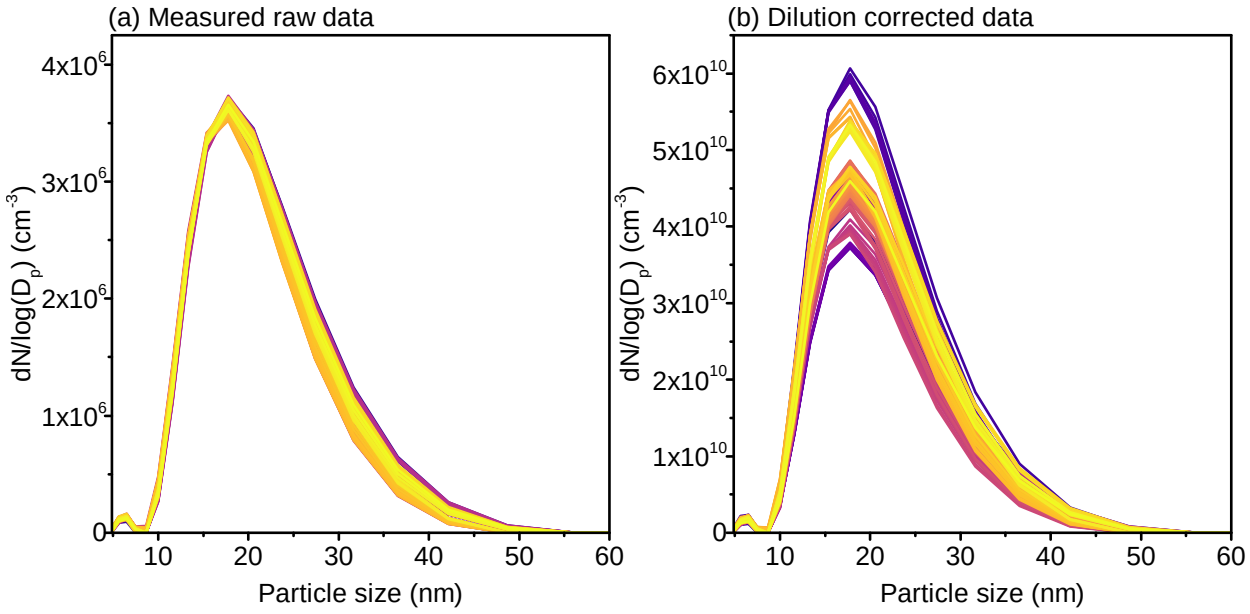

Figure S5: Particle size distribution in the centre of a heptane flame at 22 mm HAB. The as-measured data shown in (a) was corrected for N_2 dilution in (b).

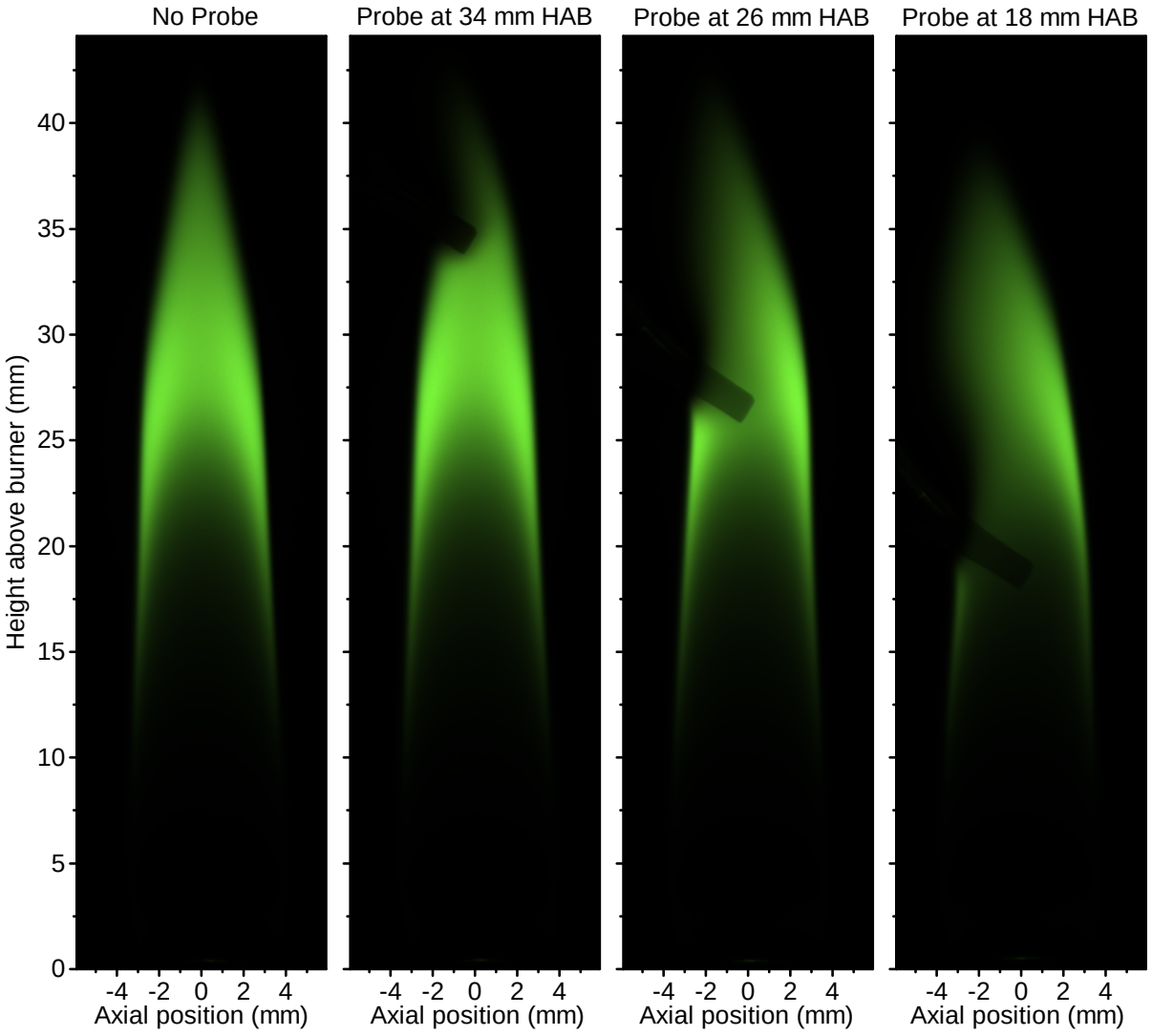

Figure S6: Original photographs used for obtaining the soot temperature and volume fraction shown in Fig. 8. The images were taken with a FGB39 filter and identical exposure times.

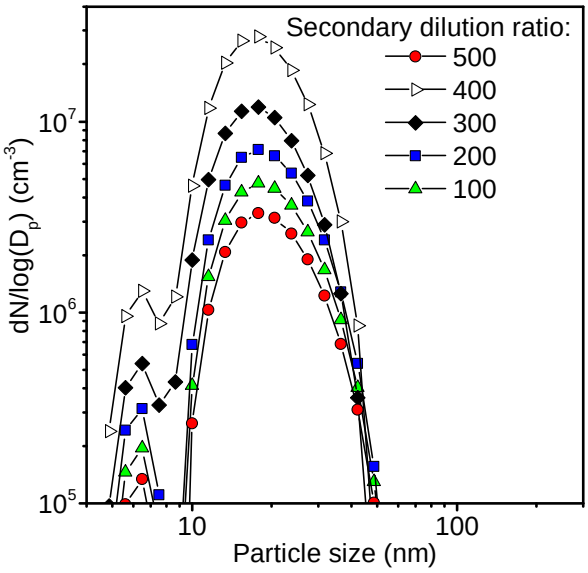

Figure S7: Raw particle size distribution measured in the 85% heptane 15% toluene flame at 16 mm HAB while varying the secondary dilution factor.

Table S1: Averaged measured soot particle size distributions along the centreline of the heptane flame in dN/dlogD_p (cm^{-3}).

	HAB (mm)										
D_p (nm)	10	11	12	13	14	15	16	17	18	19	20
4.87	9.1044E+07	9.4909E+07	9.3828E+07	2.4625E+08	4.5570E+08	6.3897E+08	6.6337E+08	6.5728E+08	5.1116E+08	2.2908E+08	2.2965E+08
5.62	1.0898E+08	1.1172E+08	1.1019E+08	3.6486E+08	7.8661E+08	1.6244E+09	1.9674E+09	1.8228E+09	1.5938E+09	6.9696E+08	4.6650E+08
6.49	9.5710E+07	9.1974E+07	8.8019E+07	3.3408E+08	8.2806E+08	2.3943E+09	3.4800E+09	3.6745E+09	3.4815E+09	2.2356E+09	1.8336E+09
7.5	8.3543E+07	7.9767E+07	6.7290E+07	2.3366E+08	6.1851E+08	2.4601E+09	4.6155E+09	6.1154E+09	7.0765E+09	6.7517E+09	6.6202E+09
8.66	6.1847E+07	5.7982E+07	4.1010E+07	1.1630E+08	3.1289E+08	1.8677E+09	4.9792E+09	8.3055E+09	1.1359E+10	1.3110E+10	1.4280E+10
10	5.9074E+07	5.4586E+07	3.5342E+07	4.8477E+07	9.1200E+07	1.0573E+09	4.4580E+09	9.0942E+09	1.4342E+10	1.8607E+10	2.2386E+10
11.55	6.4747E+07	5.9947E+07	3.6083E+07	3.2057E+07	1.7910E+07	4.3711E+08	3.2431E+09	7.9300E+09	1.4589E+10	2.0937E+10	2.8203E+10
13.34	6.2672E+07	5.8496E+07	2.8987E+07	2.7950E+07	1.2058E+07	1.2160E+08	1.8006E+09	5.4127E+09	1.2301E+10	1.9695E+10	3.0070E+10
15.4	6.0673E+07	5.6862E+07	2.4585E+07	2.8008E+07	1.3251E+07	2.5181E+07	6.5160E+08	2.7111E+09	8.6874E+09	1.5834E+10	2.7548E+10
17.78	5.6324E+07	5.1658E+07	2.1103E+07	2.7250E+07	1.5483E+07	9.0183E+06	8.9182E+07	8.7606E+08	5.1144E+09	1.0881E+10	2.1487E+10
20.54	4.7428E+07	4.0904E+07	1.5028E+07	2.2924E+07	1.3786E+07	9.9161E+06	4.8499E+06	1.0575E+08	2.4051E+09	6.2571E+09	1.4049E+10
23.71	3.8428E+07	3.1160E+07	1.1014E+07	1.8588E+07	1.1390E+07	9.9394E+06	3.7241E+06	5.6478E+06	7.8135E+08	2.9281E+09	7.5930E+09
27.38	3.0936E+07	2.4876E+07	9.0827E+06	1.4959E+07	9.2114E+06	9.0408E+06	3.3806E+06	4.1035E+06	1.2341E+08	9.4620E+08	3.2282E+09
31.62	2.6386E+07	2.1977E+07	8.8008E+06	1.2748E+07	7.8862E+06	8.2109E+06	5.0652E+06	3.8501E+06	2.4989E+06	9.9617E+07	8.7922E+08
36.52	2.3805E+07	2.0911E+07	8.8951E+06	1.1210E+07	7.2982E+06	7.5953E+06	7.8930E+06	4.5124E+06	4.4513E+06	1.2434E+06	4.6252E+07
42.17	2.2298E+07	2.0650E+07	9.2600E+06	1.0329E+07	7.3655E+06	7.1477E+06	1.0127E+07	5.9437E+06	5.5526E+06	3.5466E+06	7.9739E+06
48.7	2.1594E+07	2.0310E+07	9.6503E+06	9.8706E+06	7.5792E+06	6.7240E+06	1.0532E+07	7.2130E+06	5.6805E+06	5.4414E+06	9.1478E+06
56.23	2.0983E+07	1.9577E+07	9.8904E+06	1.0028E+07	7.5996E+06	6.5062E+06	9.8212E+06	7.4958E+06	6.2354E+06	5.9066E+06	1.0196E+07
64.94	2.0035E+07	1.8457E+07	9.6202E+06	1.0163E+07	7.2093E+06	6.3573E+06	8.7613E+06	6.6537E+06	7.2029E+06	5.2436E+06	1.0753E+07
74.99	1.8390E+07	1.6534E+07	8.6215E+06	9.8919E+06	6.5417E+06	5.9706E+06	7.6799E+06	5.2876E+06	7.6675E+06	4.8510E+06	9.9341E+06
86.6	1.6237E+07	1.4228E+07	7.3182E+06	8.9374E+06	5.5631E+06	5.2770E+06	6.7572E+06	4.4569E+06	6.9582E+06	4.8947E+06	8.4760E+06
100	1.3896E+07	1.1925E+07	5.9704E+06	7.4852E+06	4.6222E+06	4.4905E+06	5.9243E+06	4.0467E+06	5.3590E+06	4.2084E+06	6.9780E+06
115.48	1.1577E+07	9.8364E+06	4.7768E+06	5.9000E+06	3.8644E+06	3.6380E+06	4.9887E+06	3.8679E+06	3.9270E+06	2.9010E+06	5.8322E+06
133.35	9.4308E+06	7.9176E+06	3.7688E+06	4.4995E+06	3.1953E+06	2.8504E+06	4.0276E+06	3.4445E+06	3.2916E+06	2.3879E+06	4.7705E+06
153.99	7.3875E+06	6.1812E+06	2.9675E+06	3.4219E+06	2.5069E+06	2.2316E+06	3.1650E+06	2.6815E+06	2.8093E+06	2.3845E+06	3.9778E+06
177.83	5.5109E+06	4.6610E+06	2.3618E+06	2.6434E+06	1.8474E+06	1.8051E+06	2.4436E+06	1.8859E+06	2.3677E+06	2.4719E+06	3.2773E+06
205.35	4.0886E+06	3.5073E+06	1.8587E+06	2.0635E+06	1.3214E+06	1.4520E+06	1.8796E+06	1.3184E+06	1.8837E+06	2.2839E+06	2.7184E+06
237.14	3.2284E+06	2.7100E+06	1.4076E+06	1.6169E+06	9.7375E+05	1.1144E+06	1.5005E+06	9.7032E+05	1.4416E+06	1.8658E+06	2.1623E+06
273.84	2.7739E+06	2.1457E+06	1.0741E+06	1.2833E+06	7.6851E+05	8.2912E+05	1.2404E+06	7.5761E+05	1.0838E+06	1.3957E+06	1.6525E+06
316.23	2.4842E+06	1.7427E+06	8.3851E+05	1.0238E+06	6.3247E+05	6.1896E+05	1.0329E+06	6.1561E+05	8.8893E+05	1.0235E+06	1.2364E+06
365.17	2.1677E+06	1.4112E+06	6.7706E+05	8.2356E+05	5.3274E+05	4.8118E+05	8.4550E+05	5.1907E+05	7.7255E+05	7.8824E+05	9.3883E+05
421.7	1.7870E+06	1.1294E+06	5.7282E+05	6.5445E+05	4.4262E+05	3.8397E+05	6.7214E+05	4.4134E+05	6.6024E+05	6.4004E+05	7.3234E+05
486.97	1.3888E+06	8.8331E+05	5.0667E+05	5.0444E+05	3.5528E+05	3.1243E+05	5.1650E+05	3.7054E+05	5.5191E+05	5.2121E+05	5.8779E+05
562.34	1.0515E+06	6.7105E+05	4.5500E+05	3.8862E+05	2.8856E+05	2.7332E+05	3.8592E+05	3.0865E+05	4.4744E+05	4.1499E+05	4.6069E+05
649.38	8.4648E+05	5.2221E+05	4.2676E+05	3.1569E+05	2.4378E+05	2.5254E+05	3.0527E+05	2.6335E+05	3.5180E+05	3.3449E+05	3.7254E+05
749.89	7.8635E+05	4.4249E+05	4.1130E+05	2.8069E+05	2.2131E+05	2.4140E+05	2.6983E+05	2.3813E+05	2.8876E+05	2.9256E+05	3.4260E+05
865.96	8.2392E+05	4.1870E+05	3.9556E+05	2.7130E+05	2.0732E+05	2.2229E+05	2.5988E+05	2.2752E+05	2.5704E+05	2.8159E+05	3.5837E+05
1000	9.2829E+05	4.5874E+05	3.8330E+05	2.7878E+05	1.9057E+05	1.9757E+05	2.5547E+05	2.1629E+05	2.5392E+05	2.8385E+05	4.1581E+05

	HAB (mm)										
dN/dlogD_p (nm)	21	22	23	24	25	26	27	28	29	30	31
4.87	2.5255E+08	3.4230E+08	3.2966E+08	2.3339E+08	1.6321E+08	1.5076E+08	4.5997E+07	8.6046E+07	8.0102E+07	3.9431E+08	3.8587E+07
5.62	4.7265E+08	1.0074E+09	1.2331E+09	9.2682E+08	7.1089E+08	6.2079E+08	1.0836E+08	1.7979E+08	1.3043E+08	6.0054E+08	4.8292E+07
6.49	8.1064E+08	1.3007E+09	1.4701E+09	1.1355E+09	9.2826E+08	8.4976E+08	1.6852E+08	2.3016E+08	1.3353E+08	5.2619E+08	4.8881E+07
7.5	3.4251E+09	1.3567E+09	3.8825E+08	1.9491E+08	1.3268E+08	1.3440E+08	8.0755E+07	6.6765E+07	3.4234E+07	2.4798E+08	3.1877E+07
8.66	9.0658E+09	3.4996E+09	3.4026E+08	3.4847E+06	2.0452E+05	0.0000E+00	0.0000E+00	0.0000E+00	0.0000E+00	0.0000E+00	0.0000E+00
10	1.7493E+10	1.0604E+10	4.2288E+09	2.3484E+09	1.1924E+09	3.2583E+08	6.2176E+06	0.0000E+00	0.0000E+00	6.9865E+05	0.0000E+00
11.55	2.6964E+10	2.3235E+10	1.5231E+10	1.1706E+10	9.7618E+09	8.5199E+09	1.9457E+09	2.5657E+09	1.0906E+09	6.2608E+08	6.2517E+07
13.34	3.4386E+10	3.7196E+10	3.0323E+10	2.6427E+10	2.4305E+10	2.3572E+10	6.4487E+09	7.9888E+09	3.6612E+09	2.4976E+09	1.0129E+09
15.4	3.6747E+10	4.6507E+10	4.3680E+10	4.1339E+10	4.0244E+10	4.1413E+10	1.2966E+10	1.4550E+10	5.9802E+09	4.0650E+09	2.0190E+09
17.78	3.2848E+10	4.7138E+10	5.0297E+10	5.1205E+10	5.2523E+10	5.7009E+10	2.0404E+10	2.0387E+10	6.4858E+09	3.8231E+09	2.0914E+09
20.54	2.4715E+10	4.0142E+10	4.9261E+10	5.4031E+10	5.8501E+10	6.6945E+10	2.7757E+10	2.5239E+10	5.7876E+09	2.1205E+09	1.1857E+09
23.71	1.5847E+10	2.9554E+10	4.2604E+10	5.0548E+10	5.7875E+10	6.9800E+10	3.4193E+10	2.9837E+10	5.8495E+09	6.8401E+08	0.0000E+00
27.38	8.5956E+09	1.8920E+10	3.3097E+10	4.2790E+10	5.1989E+10	6.6178E+10	3.8884E+10	3.4436E+10	8.1782E+09	1.4579E+09	0.0000E+00
31.62	3.7306E+09	1.0316E+10	2.3184E+10	3.3083E+10	4.2932E+10	5.7915E+10	4.1134E+10	3.8625E+10	1.3299E+10	5.6535E+09	1.3663E+09
36.52	1.2306E+09	4.6551E+09	1.4548E+10	2.3301E+10	3.2605E+10	4.6935E+10	4.0773E+10	4.1810E+10	2.0444E+10	1.3139E+10	5.5288E+09
42.17	1.9755E+08	1.7478E+09	8.0835E+09	1.4810E+10	2.2649E+10	3.5174E+10	3.7871E+10	4.3266E+10	2.8266E+10	2.2877E+10	1.2347E+10
48.7	1.5413E+07	4.7256E+08	3.9790E+09	8.4298E+09	1.4322E+10	2.4356E+10	3.2700E+10	4.2262E+10	3.5099E+10	3.3242E+10	2.1074E+10
56.23	3.2842E+06	6.3203E+07	1.7934E+09	4.2773E+09	8.1952E+09	1.5540E+10	2.6011E+10	3.8339E+10	3.8718E+10	4.1204E+10	2.9361E+10
64.94	7.7489E+06	3.0855E+06	7.4655E+08	1.9697E+09	4.2298E+09	9.1013E+09	1.8821E+10	3.1810E+10	3.7801E+10	4.4236E+10	3.4665E+10
74.99	1.2196E+07	1.2623E+06	2.4583E+08	8.5597E+08	1.9762E+09	4.8619E+09	1.2174E+10	2.3654E+10	3.2280E+10	4.1128E+10	3.5157E+10
86.6	1.3590E+07	6.0680E+06	5.8472E+07	3.1901E+08	8.1584E+08	2.3388E+09	6.8597E+09	1.5353E+10	2.3682E+10	3.2814E+10	3.0622E+10
100	1.1594E+07	1.1871E+07	1.3987E+07	9.2583E+07	2.7559E+08	9.6333E+08	3.2249E+09	8.3536E+09	1.4475E+10	2.1995E+10	2.2617E+10
115.48	8.0114E+06	1.3083E+07	1.6556E+07	2.6605E+07	7.9740E+07	3.2938E+08	1.1597E+09	3.5217E+09	6.9382E+09	1.1851E+10	1.3742E+10
133.35	5.3188E+06	9.9696E+06	1.9981E+07	1.5968E+07	2.7115E+07	9.3772E+07	2.5130E+08	9.3212E+08	2.2589E+09	4.6516E+09	6.4288E+09
153.99	4.0733E+06	5.7934E+06	1.5160E+07	1.4999E+07	1.8603E+07	3.3212E+07	2.9893E+06	1.7112E+07	2.8088E+08	9.8744E+08	1.9573E+09
177.83	3.7633E+06	3.3093E+06	7.2043E+06	1.0996E+07	1.4864E+07	1.7899E+07	1.0580E+07	9.6162E+05	0.0000E+00	0.0000E+00	1.6298E+08
205.35	3.5297E+06	2.6435E+06	2.2895E+06	5.5446E+06	9.8523E+06	1.3884E+07	2.2439E+07	6.5440E+06	0.0000E+00	0.0000E+00	0.0000E+00
237.14	3.0911E+06	2.8615E+06	1.2725E+06	2.0995E+06	5.3055E+06	1.1649E+07	2.5127E+07	1.4845E+07	7.0159E+04	0.0000E+00	0.0000E+00
273.84	2.5237E+06	2.9732E+06	1.7413E+06	9.8634E+05	1.7812E+06	7.2808E+06	1.7321E+07	1.4542E+07	5.0947E+05	5.0471E+06	0.0000E+00
316.23	1.9871E+06	2.7349E+06	2.0855E+06	1.3316E+06	5.2640E+05	2.8740E+06	8.3174E+06	1.0567E+07	1.6682E+06	1.1615E+07	0.0000E+00
365.17	1.5347E+06	2.2121E+06	2.0380E+06	1.5220E+06	5.9573E+05	6.8734E+05	2.6804E+06	5.9849E+06	2.9152E+06	1.5771E+07	0.0000E+00
421.7	1.1451E+06	1.5850E+06	1.6535E+06	1.4085E+06	6.5219E+05	4.3300E+05	6.8294E+05	2.5473E+06	2.8282E+06	1.3638E+07	0.0000E+00
486.97	8.2294E+05	1.0171E+06	1.1294E+06	1.1459E+06	6.0716E+05	4.6925E+05	1.0085E+04	5.1669E+05	1.1749E+06	6.6831E+06	2.3325E+04
562.34	5.6118E+05	5.9392E+05	6.7937E+05	9.0681E+05	5.1787E+05	4.2539E+05	1.9460E+04	0.0000E+00	0.0000E+00	1.9139E+03	3.4168E+04
649.38	3.8666E+05	3.4690E+05	3.9309E+05	7.6567E+05	4.3435E+05	3.6532E+05	5.2193E+04	1.5889E+04	0.0000E+00	0.0000E+00	0.0000E+00
749.89	3.2276E+05	2.8476E+05	3.2167E+05	7.2019E+05	3.8275E+05	3.2368E+05	1.0986E+05	1.1080E+05	0.0000E+00	0.0000E+00	0.0000E+00
865.96	3.6656E+05	3.6615E+05	3.7556E+05	7.2786E+05	3.7057E+05	3.0173E+05	1.8869E+05	2.5228E+05	0.0000E+00	0.0000E+00	0.0000E+00
1000	5.0929E+05	5.6873E+05	5.4179E+05	7.7281E+05	3.7408E+05	2.9500E+05	2.3966E+05	4.1085E+05	3.5649E+05	2.3422E+06	0.0000E+00

	HAB (mm)								
D_p (nm)	32	33	34	35	36	37	38	39	40
4.87	4.9644E+07	3.3701E+07	3.2681E+07	9.0203E+07	3.5729E+07	2.2481E+07	3.8238E+07	2.0300E+08	6.5385E+07
5.62	6.2019E+07	4.1439E+07	3.8983E+07	1.2819E+08	4.4983E+07	2.8470E+07	5.4205E+07	2.9661E+08	9.3117E+07
6.49	6.2182E+07	4.5527E+07	4.2351E+07	1.1857E+08	4.8239E+07	2.8994E+07	6.6654E+07	3.3483E+08	1.3945E+08
7.5	4.3445E+07	3.4737E+07	3.1951E+07	6.8653E+07	3.5140E+07	2.0853E+07	4.4847E+07	2.4018E+08	1.9769E+08
8.66	0.0000E+00	0.0000E+00	3.3579E+05	2.9510E+06	8.6929E+05	3.8403E+05	2.1943E+05	1.2237E+08	3.4292E+08
10	0.0000E+00	0.0000E+00	0.0000E+00	5.4152E+04	0.0000E+00	0.0000E+00	1.1844E+06	3.8597E+08	7.4293E+08
11.55	5.0071E+06	1.0469E+06	9.7945E+05	2.6053E+07	5.1100E+06	1.3646E+07	1.9174E+08	1.5903E+09	1.4238E+09
13.34	6.4250E+08	4.1948E+08	3.1441E+08	3.7093E+08	3.2162E+08	3.7200E+08	7.8039E+08	3.3722E+09	2.2420E+09
15.4	1.6448E+09	1.2618E+09	1.0108E+09	1.0491E+09	9.4722E+08	9.5094E+08	1.3693E+09	4.8461E+09	2.9837E+09
17.78	2.2644E+09	1.9564E+09	1.6378E+09	1.6381E+09	1.4584E+09	1.2681E+09	1.5148E+09	5.4002E+09	3.4892E+09
20.54	1.9984E+09	1.9271E+09	1.6709E+09	1.6462E+09	1.4338E+09	1.0648E+09	1.2057E+09	5.3989E+09	3.7478E+09
23.71	8.8642E+08	1.0114E+09	9.1268E+08	8.9600E+08	7.6055E+08	4.5329E+08	8.1487E+08	5.7414E+09	3.8309E+09
27.38	0.0000E+00	0.0000E+00	0.0000E+00	6.0080E+06	2.8487E+07	5.6146E+07	8.9347E+08	7.0622E+09	3.7753E+09
31.62	4.0311E+08	1.1180E+08	1.3161E+07	3.4748E+07	1.2288E+08	5.2998E+08	1.8998E+09	9.4988E+09	3.5780E+09
36.52	3.3502E+09	2.1904E+09	1.4862E+09	1.3804E+09	1.5720E+09	2.2585E+09	3.8119E+09	1.2685E+10	3.2607E+09
42.17	8.9988E+09	6.5841E+09	4.9948E+09	4.6785E+09	4.7031E+09	5.2758E+09	6.4187E+09	1.6019E+10	2.8329E+09
48.7	1.6918E+10	1.3110E+10	1.0582E+10	1.0035E+10	9.4508E+09	9.3523E+09	9.3640E+09	1.8782E+10	2.2986E+09
56.23	2.5199E+10	2.0337E+10	1.7144E+10	1.6437E+10	1.4828E+10	1.3546E+10	1.1887E+10	2.0083E+10	1.7075E+09
64.94	3.1439E+10	2.6243E+10	2.2890E+10	2.2151E+10	1.9351E+10	1.6663E+10	1.3236E+10	1.9396E+10	1.1328E+09
74.99	3.3618E+10	2.8968E+10	2.6039E+10	2.5409E+10	2.1604E+10	1.7696E+10	1.2927E+10	1.6706E+10	6.5009E+08
86.6	3.0966E+10	2.7572E+10	2.5510E+10	2.5092E+10	2.0802E+10	1.6258E+10	1.0997E+10	1.2628E+10	3.0706E+08
100	2.4394E+10	2.2522E+10	2.1470E+10	2.1284E+10	1.7199E+10	1.2809E+10	8.0220E+09	8.1776E+09	1.0879E+08
115.48	1.6094E+10	1.5515E+10	1.5289E+10	1.5282E+10	1.2004E+10	8.4633E+09	4.8661E+09	4.3484E+09	2.3345E+07
133.35	8.5137E+09	8.6800E+09	8.8997E+09	8.9779E+09	6.8165E+09	4.4782E+09	2.3031E+09	1.7374E+09	1.7813E+06
153.99	3.2773E+09	3.6239E+09	3.9121E+09	3.9897E+09	2.8979E+09	1.7107E+09	7.2798E+08	4.0925E+08	9.7444E+05
177.83	6.9304E+08	8.8805E+08	1.0371E+09	1.0736E+09	7.2902E+08	3.4214E+08	7.5162E+07	2.8981E+06	1.3578E+06
205.35	0.0000E+00	0.0000E+00	0.0000E+00	0.0000E+00	0.0000E+00	0.0000E+00	0.0000E+00	2.4486E+05	1.3492E+06
237.14	0.0000E+00	0.0000E+00	0.0000E+00	0.0000E+00	0.0000E+00	0.0000E+00	0.0000E+00	9.3863E+05	1.0510E+06
273.84	0.0000E+00	0.0000E+00	0.0000E+00	0.0000E+00	0.0000E+00	0.0000E+00	0.0000E+00	1.4132E+06	7.4977E+05
316.23	0.0000E+00	0.0000E+00	0.0000E+00	0.0000E+00	0.0000E+00	0.0000E+00	0.0000E+00	1.6333E+06	5.5110E+05
365.17	0.0000E+00	0.0000E+00	0.0000E+00	0.0000E+00	0.0000E+00	0.0000E+00	1.9590E+04	1.8555E+06	4.4395E+05
421.7	0.0000E+00	0.0000E+00	0.0000E+00	6.1301E+03	0.0000E+00	0.0000E+00	1.5338E+05	2.3110E+06	3.6075E+05
486.97	0.0000E+00	0.0000E+00	0.0000E+00	2.4512E+05	0.0000E+00	1.5966E+03	2.6317E+05	2.0515E+06	2.9659E+05
562.34	0.0000E+00	2.5031E+03	6.0383E+03	5.5462E+05	3.8062E+02	4.9957E+03	1.9249E+05	1.0549E+06	2.7118E+05
649.38	9.4175E+02	8.4659E+03	1.3465E+04	4.6795E+05	6.8719E+03	7.3390E+03	4.0603E+03	1.7717E+05	2.5526E+05
749.89	0.0000E+00	0.0000E+00	0.0000E+00	0.0000E+00	0.0000E+00	0.0000E+00	0.0000E+00	2.1508E+05	2.3198E+05
865.96	0.0000E+00	0.0000E+00	0.0000E+00	0.0000E+00	0.0000E+00	0.0000E+00	0.0000E+00	3.7454E+05	1.9348E+05
1000	0.0000E+00	0.0000E+00	0.0000E+00	0.0000E+00	0.0000E+00	0.0000E+00	8.3975E+03	6.3919E+05	1.6277E+05

Table S2: Averaged measured soot particle size distributions along the centreline of the 5 mol% toluene/heptane flame in dN/dlogD_p (cm^{-3}).

	HAB (mm)										
D_p (nm)	10	11	12	13	14	15	16	17	18	19	20
4.87	2.6610E+08	5.4392E+08	1.0140E+09	7.4898E+08	2.3610E+08	1.5545E+08	1.8158E+08	2.7060E+08	3.4126E+08	4.7434E+08	3.7734E+08
5.62	4.3008E+08	9.7341E+08	2.6869E+09	2.7331E+09	7.7377E+08	4.0605E+07	4.9856E+06	1.6593E+08	8.0178E+08	1.5939E+09	1.4529E+09
6.49	4.4709E+08	1.0686E+09	4.1247E+09	5.5750E+09	3.1260E+09	1.2395E+09	2.2888E+08	3.8676E+08	1.0361E+09	1.8593E+09	1.7226E+09
7.5	3.5790E+08	8.4657E+08	4.5070E+09	8.3499E+09	8.7811E+09	8.0039E+09	5.3104E+09	3.6118E+09	1.7532E+09	8.3849E+08	3.8250E+08
8.66	2.1194E+08	4.7284E+08	3.8183E+09	1.0016E+10	1.5793E+10	1.8498E+10	1.4633E+10	1.0959E+10	5.2761E+09	1.7123E+09	1.3442E+08
10	1.0094E+08	1.7224E+08	2.6172E+09	9.8043E+09	2.0337E+10	2.7526E+10	2.4978E+10	2.2110E+10	1.4062E+10	9.0106E+09	4.5877E+09
11.55	5.4961E+07	4.9159E+07	1.4939E+09	7.7060E+09	1.9866E+10	3.0707E+10	3.2576E+10	3.4648E+10	2.7720E+10	2.4123E+10	1.7352E+10
13.34	4.4601E+07	3.0929E+07	6.8815E+08	4.6672E+09	1.5203E+10	2.7632E+10	3.5102E+10	4.4251E+10	4.1533E+10	4.2101E+10	3.4840E+10
15.4	4.5093E+07	3.1149E+07	2.0943E+08	1.9608E+09	9.0753E+09	2.0582E+10	3.1916E+10	4.6745E+10	4.9433E+10	5.5372E+10	5.0045E+10
17.78	4.4782E+07	3.3296E+07	1.9489E+07	4.4716E+08	4.1456E+09	1.2648E+10	2.4160E+10	4.0584E+10	4.7751E+10	5.8437E+10	5.7013E+10
20.54	3.9207E+07	3.0728E+07	1.1131E+07	2.9333E+07	1.3483E+09	6.1278E+09	1.4794E+10	2.8876E+10	3.8323E+10	5.1830E+10	5.4853E+10
23.71	3.2524E+07	2.6696E+07	1.1301E+07	8.8883E+05	2.9096E+08	2.1219E+09	7.0362E+09	1.6778E+10	2.6008E+10	3.9848E+10	4.6255E+10
27.38	2.6560E+07	2.2891E+07	1.0392E+07	1.6443E+06	1.9978E+07	4.1465E+08	2.3121E+09	7.5848E+09	1.4721E+10	2.6715E+10	3.4667E+10
31.62	2.2831E+07	2.0513E+07	1.1060E+07	4.8146E+06	4.7903E+04	5.2112E+06	2.5623E+08	2.1659E+09	6.4510E+09	1.5291E+10	2.3009E+10
36.52	2.0265E+07	1.8771E+07	1.2414E+07	9.4949E+06	2.8169E+06	4.1769E+05	0.0000E+00	1.2708E+08	1.8278E+09	7.1323E+09	1.3236E+10
42.17	1.8483E+07	1.7652E+07	1.2950E+07	1.3114E+07	7.9175E+06	1.1889E+06	0.0000E+00	0.0000E+00	1.7781E+08	2.4657E+09	6.3021E+09
48.7	1.7656E+07	1.7101E+07	1.2731E+07	1.4285E+07	1.2659E+07	2.8085E+06	2.5778E+05	0.0000E+00	0.0000E+00	5.1038E+08	2.2901E+09
56.23	1.7392E+07	1.6686E+07	1.2085E+07	1.3507E+07	1.5582E+07	7.3735E+06	1.4690E+06	1.8732E+05	0.0000E+00	2.5540E+07	5.4022E+08
64.94	1.7171E+07	1.5791E+07	1.1328E+07	1.1516E+07	1.5605E+07	1.3372E+07	5.9613E+06	2.3275E+06	2.2734E+04	7.4552E+05	3.0695E+07
74.99	1.6308E+07	1.4173E+07	1.0418E+07	9.4357E+06	1.3335E+07	1.7254E+07	1.2621E+07	7.5256E+06	1.2292E+06	6.2290E+05	0.0000E+00
86.6	1.4501E+07	1.1989E+07	8.9341E+06	7.9808E+06	1.0700E+07	1.6629E+07	1.5988E+07	1.3644E+07	4.4670E+06	3.9804E+06	8.0746E+05
100	1.2113E+07	9.8246E+06	7.0810E+06	6.9348E+06	8.4351E+06	1.2504E+07	1.3530E+07	1.5315E+07	8.0097E+06	8.6415E+06	8.0683E+06
115.48	9.5177E+06	7.9808E+06	5.3977E+06	5.8083E+06	6.9200E+06	8.1044E+06	7.7587E+06	1.0992E+07	8.5309E+06	1.1370E+07	1.1881E+07
133.35	7.3246E+06	6.4415E+06	4.1571E+06	4.5497E+06	5.7699E+06	6.1470E+06	4.0512E+06	4.6619E+06	5.4548E+06	1.0282E+07	1.1040E+07
153.99	5.6836E+06	4.9603E+06	3.2795E+06	3.2766E+06	4.7377E+06	5.2459E+06	3.4931E+06	2.6335E+06	2.0259E+06	6.5015E+06	7.1800E+06
177.83	4.4379E+06	3.6917E+06	2.6542E+06	2.2648E+06	3.7326E+06	4.5811E+06	3.9439E+06	2.8641E+06	1.2548E+06	3.2349E+06	3.0788E+06
205.35	3.5417E+06	2.7315E+06	2.1176E+06	1.6385E+06	2.8609E+06	3.8469E+06	4.3214E+06	4.1445E+06	1.8501E+06	2.2181E+06	1.1002E+06
237.14	2.8421E+06	2.0910E+06	1.7063E+06	1.3519E+06	2.1921E+06	3.0713E+06	4.0740E+06	4.7938E+06	2.9349E+06	2.4334E+06	9.8916E+05
273.84	2.2926E+06	1.6882E+06	1.3970E+06	1.2169E+06	1.7649E+06	2.4304E+06	3.4187E+06	4.5004E+06	3.3848E+06	3.1042E+06	1.5648E+06
316.23	1.8681E+06	1.4479E+06	1.1400E+06	1.0749E+06	1.5495E+06	1.9927E+06	2.6632E+06	3.6332E+06	3.0606E+06	3.3643E+06	2.2955E+06
365.17	1.5414E+06	1.2512E+06	8.9117E+05	8.7855E+05	1.3669E+06	1.6926E+06	1.9973E+06	2.6662E+06	2.3183E+06	2.9961E+06	2.5141E+06
421.7	1.3005E+06	1.0489E+06	6.8434E+05	6.9275E+05	1.1251E+06	1.4100E+06	1.4593E+06	1.8644E+06	1.5563E+06	2.2626E+06	2.1696E+06
486.97	1.1023E+06	8.3485E+05	5.1885E+05	5.5988E+05	8.5862E+05	1.1300E+06	1.0763E+06	1.2872E+06	9.9144E+05	1.5108E+06	1.5437E+06
562.34	9.3473E+05	6.2901E+05	4.1400E+05	4.6716E+05	6.3611E+05	8.7598E+05	8.2135E+05	8.9815E+05	6.4569E+05	9.4627E+05	9.5363E+05
649.38	7.9302E+05	4.8301E+05	3.5049E+05	3.9573E+05	5.0249E+05	6.9485E+05	6.5954E+05	6.8642E+05	4.8995E+05	6.0694E+05	5.6784E+05
749.89	6.9999E+05	4.1180E+05	3.2052E+05	3.4909E+05	4.4880E+05	6.0553E+05	5.8069E+05	6.1256E+05	4.6952E+05	4.8112E+05	4.1584E+05
865.96	6.6605E+05	3.9084E+05	2.9877E+05	3.1871E+05	4.3780E+05	5.8499E+05	5.7337E+05	6.3814E+05	5.1305E+05	5.0937E+05	4.0538E+05
1000	6.9026E+05	4.0580E+05	3.0433E+05	3.0818E+05	4.6387E+05	6.2015E+05	6.5208E+05	7.7813E+05	6.1646E+05	7.0225E+05	5.1370E+05

	HAB (mm)										
D_p (nm)	21	22	23	24	25	26	27	28	29	30	31
4.87	2.8673E+08	1.5456E+08	1.5992E+08	1.1907E+08	1.1213E+08	7.6868E+07	7.8152E+07	6.7329E+07	5.1647E+07	5.8523E+07	6.3389E+07
5.62	1.0670E+09	6.6396E+08	5.7902E+08	3.2722E+08	2.2822E+08	1.5292E+08	1.2729E+08	9.7961E+07	7.0032E+07	8.0076E+07	8.5615E+07
6.49	1.3004E+09	9.0356E+08	7.9794E+08	4.7142E+08	3.0008E+08	2.0841E+08	1.3721E+08	1.0672E+08	7.9714E+07	8.3428E+07	8.5451E+07
7.5	2.3385E+08	1.6631E+08	2.2494E+08	2.4858E+08	1.8422E+08	1.1044E+08	4.8509E+07	5.6949E+07	5.7434E+07	5.6950E+07	5.8269E+07
8.66	1.7472E+06	0.0000E+00	0.0000E+00	2.3570E+06	1.1968E+07	2.9102E+06	0.0000E+00	0.0000E+00	0.0000E+00	9.3786E+05	2.2824E+06
10	2.1753E+09	5.4208E+08	2.9696E+08	8.9645E+07	1.5053E+08	9.1196E+07	0.0000E+00	0.0000E+00	0.0000E+00	0.0000E+00	0.0000E+00
11.55	1.2523E+10	8.6467E+09	6.9476E+09	3.5512E+09	2.2057E+09	1.9837E+09	1.1385E+09	3.8123E+08	3.9093E+07	1.2841E+06	9.2851E+05
13.34	2.8623E+10	2.2919E+10	1.9404E+10	1.1373E+10	7.3080E+09	6.2739E+09	3.7067E+09	2.0630E+09	1.0834E+09	4.7469E+08	3.3052E+08
15.4	4.4581E+10	3.9019E+10	3.4581E+10	2.3156E+10	1.5956E+10	1.2759E+10	6.4180E+09	3.7312E+09	2.3691E+09	1.4157E+09	1.0969E+09
17.78	5.4629E+10	5.1928E+10	4.8378E+10	3.7055E+10	2.7550E+10	2.0800E+10	8.0790E+09	3.9149E+09	2.7719E+09	2.2179E+09	1.8437E+09
20.54	5.6735E+10	5.8632E+10	5.7573E+10	4.9949E+10	4.0014E+10	2.9664E+10	9.0658E+09	2.7121E+09	1.9647E+09	2.2129E+09	1.9373E+09
23.71	5.1927E+10	5.8323E+10	6.0437E+10	5.8690E+10	5.0687E+10	3.8489E+10	1.0688E+10	1.5271E+09	4.8204E+08	1.1750E+09	1.0856E+09
27.38	4.2668E+10	5.2208E+10	5.7251E+10	6.1750E+10	5.7491E+10	4.5983E+10	1.3807E+10	2.1810E+09	2.2811E+06	0.0000E+00	0.0000E+00
31.62	3.1680E+10	4.2567E+10	4.9643E+10	5.9220E+10	5.9346E+10	5.0766E+10	1.8474E+10	5.9921E+09	1.3864E+09	1.1267E+08	3.1752E+06
36.52	2.1043E+10	3.1469E+10	3.9408E+10	5.2087E+10	5.6349E+10	5.2212E+10	2.3979E+10	1.2688E+10	5.9932E+09	2.5008E+09	1.4671E+09
42.17	1.2216E+10	2.0812E+10	2.8450E+10	4.1954E+10	4.9271E+10	5.0039E+10	2.9288E+10	2.1381E+10	1.3803E+10	7.6307E+09	5.3139E+09
48.7	6.0162E+09	1.2134E+10	1.8529E+10	3.0719E+10	3.9347E+10	4.4303E+10	3.3221E+10	3.0746E+10	2.4139E+10	1.5332E+10	1.1822E+10
56.23	2.3812E+09	6.0835E+09	1.0751E+10	2.0240E+10	2.8438E+10	3.5911E+10	3.4398E+10	3.8170E+10	3.4450E+10	2.3962E+10	1.9915E+10
64.94	7.0390E+08	2.5358E+09	5.4608E+09	1.1786E+10	1.8312E+10	2.6320E+10	3.2159E+10	4.1331E+10	4.1700E+10	3.1130E+10	2.7503E+10
74.99	1.3795E+08	8.5143E+08	2.3806E+09	5.9161E+09	1.0283E+10	1.7136E+10	2.6738E+10	3.8977E+10	4.3470E+10	3.4599E+10	3.2317E+10
86.6	7.8963E+06	2.2597E+08	8.7383E+08	2.4644E+09	4.8711E+09	9.6549E+09	1.9401E+10	3.1716E+10	3.9067E+10	3.3171E+10	3.2736E+10
100	1.1061E+07	4.8880E+07	2.5734E+08	7.9921E+08	1.8288E+09	4.5042E+09	1.1947E+10	2.1832E+10	2.9948E+10	2.7311E+10	2.8580E+10
115.48	3.2220E+07	3.4407E+07	7.7911E+07	1.8362E+08	4.7181E+08	1.5942E+09	5.9395E+09	1.2217E+10	1.9083E+10	1.8985E+10	2.1247E+10
133.35	3.3963E+07	3.9412E+07	4.8318E+07	4.3497E+07	5.3630E+07	3.3789E+08	2.1403E+09	5.0985E+09	9.5667E+09	1.0736E+10	1.3070E+10
153.99	2.2105E+07	3.1144E+07	4.3936E+07	4.5298E+07	1.2012E+07	8.3229E+06	4.0257E+08	1.2438E+09	3.3144E+09	4.5456E+09	6.2379E+09
177.83	9.3527E+06	1.5890E+07	3.2069E+07	5.2994E+07	4.3920E+07	2.1532E+06	0.0000E+00	0.0000E+00	4.8735E+08	1.1389E+09	1.9624E+09
205.35	2.5502E+06	4.5860E+06	1.6465E+07	4.0892E+07	5.6125E+07	2.0446E+07	0.0000E+00	0.0000E+00	0.0000E+00	1.4428E+06	1.7426E+08
237.14	1.4281E+06	4.6156E+05	5.5051E+06	2.1521E+07	4.1594E+07	3.4889E+07	1.8187E+05	0.0000E+00	0.0000E+00	0.0000E+00	0.0000E+00
273.84	1.7699E+06	1.0917E+05	1.0985E+06	7.1079E+06	1.9814E+07	2.9692E+07	1.6137E+06	0.0000E+00	0.0000E+00	0.0000E+00	0.0000E+00
316.23	2.4751E+06	3.0899E+05	8.3687E+05	9.6310E+05	5.2977E+06	1.6856E+07	2.7518E+06	0.0000E+00	0.0000E+00	0.0000E+00	0.0000E+00
365.17	2.8676E+06	6.1952E+05	1.3466E+06	2.3172E+05	4.8300E+05	5.8761E+06	4.2817E+06	1.8122E+04	0.0000E+00	0.0000E+00	0.0000E+00
421.7	2.6286E+06	8.1406E+05	1.5338E+06	5.1351E+05	6.4452E+04	8.5149E+05	4.6332E+06	1.0803E+05	0.0000E+00	0.0000E+00	0.0000E+00
486.97	1.9310E+06	8.0667E+05	1.3717E+06	7.6033E+05	1.6701E+05	9.7529E+03	2.5596E+06	3.4958E+05	2.3642E+04	0.0000E+00	0.0000E+00
562.34	1.1608E+06	6.6034E+05	1.0358E+06	8.4588E+05	3.6590E+05	0.0000E+00	3.9770E+04	2.1351E+05	2.8932E+04	6.5429E+03	2.6630E+04
649.38	6.2007E+05	4.8734E+05	7.2904E+05	8.4524E+05	5.8053E+05	2.2973E+04	0.0000E+00	0.0000E+00	0.0000E+00	3.3124E+04	3.7988E+04
749.89	4.0087E+05	3.6401E+05	5.5788E+05	8.0038E+05	7.3246E+05	1.3798E+05	0.0000E+00	0.0000E+00	0.0000E+00	0.0000E+00	0.0000E+00
865.96	4.3645E+05	3.1025E+05	4.9308E+05	7.6984E+05	8.1798E+05	3.0187E+05	4.8509E+03	0.0000E+00	0.0000E+00	0.0000E+00	0.0000E+00
1000	6.8137E+05	3.1659E+05	5.6023E+05	7.8385E+05	8.5680E+05	4.5876E+05	2.2157E+05	1.3221E+04	0.0000E+00	0.0000E+00	0.0000E+00

	HAB (mm)								
D_p (nm)	32	33	34	35	36	37	38	39	40
4.87	5.6949E+07	5.6645E+07	6.0415E+07	5.6248E+07	5.0065E+07	5.2806E+07	5.3703E+07	4.8402E+07	5.7395E+07
5.62	7.6635E+07	6.9446E+07	7.3143E+07	6.5596E+07	5.9853E+07	6.5197E+07	7.0076E+07	6.6969E+07	8.0169E+07
6.49	7.7224E+07	7.0095E+07	6.8160E+07	5.9641E+07	5.7889E+07	6.6503E+07	6.6415E+07	6.9118E+07	7.8697E+07
7.5	5.8522E+07	6.1090E+07	6.2112E+07	5.7722E+07	5.6349E+07	5.8027E+07	4.8503E+07	4.7515E+07	5.1706E+07
8.66	1.5649E+07	3.2221E+07	4.2188E+07	4.1266E+07	4.0234E+07	3.0541E+07	1.4936E+07	8.3217E+06	2.0131E+07
10	6.9030E+05	6.9326E+06	1.7121E+07	2.0014E+07	1.8628E+07	1.0033E+07	2.0885E+06	3.9305E+06	4.6089E+07
11.55	4.3126E+05	5.2469E+05	1.2160E+06	2.6878E+06	3.0482E+06	5.1236E+06	1.8638E+07	7.6636E+07	2.2639E+08
13.34	1.8711E+08	1.1781E+07	3.2949E+06	2.5732E+06	1.0880E+07	5.2763E+07	1.8213E+08	3.2650E+08	5.0405E+08
15.4	7.0100E+08	3.6693E+08	2.8485E+08	2.2572E+08	2.4830E+08	3.4233E+08	5.1127E+08	6.2655E+08	7.3132E+08
17.78	1.2618E+09	1.0789E+09	8.9879E+08	7.3615E+08	7.4739E+08	8.1765E+08	8.2696E+08	7.8889E+08	8.0005E+08
20.54	1.3967E+09	1.6144E+09	1.3892E+09	1.1548E+09	1.1355E+09	1.1125E+09	8.8292E+08	7.2694E+08	7.5984E+08
23.71	8.4315E+08	1.4055E+09	1.2436E+09	1.0453E+09	1.0022E+09	8.8916E+08	5.6361E+08	5.0880E+08	7.5970E+08
27.38	5.8183E+07	6.1082E+08	5.7125E+08	4.8920E+08	4.5024E+08	3.2359E+08	1.4919E+08	3.9523E+08	9.3954E+08
31.62	0.0000E+00	0.0000E+00	0.0000E+00	0.0000E+00	5.4150E+05	2.6877E+06	1.4473E+08	6.9615E+08	1.3713E+09
36.52	7.3016E+08	1.0539E+08	3.1964E+07	3.0700E+06	5.5306E+07	1.9790E+08	7.5585E+08	1.4917E+09	2.0068E+09
42.17	3.0881E+09	1.8731E+09	1.3771E+09	1.0610E+09	1.1748E+09	1.5533E+09	2.1948E+09	2.7697E+09	2.7481E+09
48.7	7.4389E+09	5.6722E+09	4.4569E+09	3.5902E+09	3.7717E+09	4.3246E+09	4.5102E+09	4.4319E+09	3.4666E+09
56.23	1.3227E+10	1.1098E+10	9.0405E+09	7.4468E+09	7.6728E+09	8.2072E+09	7.3316E+09	6.1232E+09	3.9608E+09
64.94	1.9054E+10	1.6916E+10	1.4149E+10	1.1828E+10	1.2045E+10	1.2306E+10	9.9612E+09	7.3878E+09	4.0717E+09
74.99	2.3240E+10	2.1544E+10	1.8427E+10	1.5580E+10	1.5717E+10	1.5488E+10	1.1634E+10	7.8296E+09	3.7320E+09
86.6	2.4412E+10	2.3520E+10	2.0542E+10	1.7533E+10	1.7533E+10	1.6730E+10	1.1789E+10	7.2784E+09	3.0144E+09
100	2.2142E+10	2.2163E+10	1.9764E+10	1.7014E+10	1.6861E+10	1.5588E+10	1.0343E+10	5.8838E+09	2.1075E+09
115.48	1.7198E+10	1.7931E+10	1.6348E+10	1.4187E+10	1.3920E+10	1.2445E+10	7.7608E+09	4.0605E+09	1.2364E+09
133.35	1.1193E+10	1.2232E+10	1.1436E+10	1.0005E+10	9.7018E+09	8.3430E+09	4.8446E+09	2.3069E+09	5.7267E+08
153.99	5.8275E+09	6.7657E+09	6.5230E+09	5.7566E+09	5.4984E+09	4.5004E+09	2.3727E+09	9.9720E+08	1.8179E+08
177.83	2.1891E+09	2.7821E+09	2.7963E+09	2.4933E+09	2.3320E+09	1.7784E+09	7.9298E+08	2.6470E+08	2.3333E+07
205.35	4.3310E+08	6.6308E+08	7.1342E+08	6.4540E+08	5.8327E+08	3.9184E+08	1.0350E+08	5.5536E+06	1.9755E+04
237.14	0.0000E+00	0.0000E+00	0.0000E+00	0.0000E+00	0.0000E+00	0.0000E+00	0.0000E+00	0.0000E+00	1.0228E+05
273.84	0.0000E+00	0.0000E+00	0.0000E+00	0.0000E+00	0.0000E+00	0.0000E+00	0.0000E+00	0.0000E+00	2.6911E+05
316.23	0.0000E+00	0.0000E+00	0.0000E+00	0.0000E+00	0.0000E+00	0.0000E+00	0.0000E+00	0.0000E+00	4.2110E+05
365.17	0.0000E+00	0.0000E+00	0.0000E+00	0.0000E+00	0.0000E+00	0.0000E+00	0.0000E+00	0.0000E+00	6.7084E+05
421.7	0.0000E+00	0.0000E+00	0.0000E+00	0.0000E+00	0.0000E+00	0.0000E+00	0.0000E+00	2.9299E+04	9.0611E+05
486.97	0.0000E+00	0.0000E+00	0.0000E+00	0.0000E+00	0.0000E+00	0.0000E+00	5.5925E+03	1.5624E+05	8.3987E+05
562.34	8.8054E+02	0.0000E+00	0.0000E+00	0.0000E+00	0.0000E+00	0.0000E+00	5.4188E+04	2.7477E+05	4.7655E+05
649.38	1.1478E+04	2.0236E+04	4.5967E+04	2.7660E+04	1.5263E+04	2.1377E+03	7.4999E+04	1.8896E+05	1.0734E+05
749.89	2.3258E+04	6.5763E+04	1.1987E+05	9.4384E+04	5.8838E+04	2.2221E+04	0.0000E+00	0.0000E+00	9.5882E+04
865.96	0.0000E+00	0.0000E+00	0.0000E+00	0.0000E+00	0.0000E+00	0.0000E+00	0.0000E+00	0.0000E+00	1.2483E+05
1000	0.0000E+00	0.0000E+00	0.0000E+00	0.0000E+00	0.0000E+00	0.0000E+00	0.0000E+00	5.7040E+03	2.1438E+05

Table S3: Averaged measured soot particle size distributions along the centreline of the 10 mol% toluene/heptane flame in dN/dlogD_p (cm^{-3}).

	HAB (mm)										
D_p (nm)	10	11	12	13	14	15	16	17	18	19	20
4.87	3.5054E+08	7.4079E+08	9.6481E+08	2.9731E+08	1.2010E+08	1.5889E+08	2.1988E+08	3.7303E+08	3.5298E+08	1.5684E+08	1.8641E+08
5.62	5.9723E+08	1.5365E+09	2.8486E+09	1.1166E+09	2.6075E+07	5.1973E+06	2.8140E+08	1.1320E+09	1.2880E+09	1.1116E+09	8.2142E+08
6.49	6.4746E+08	1.9518E+09	4.8066E+09	3.5950E+09	1.1168E+09	9.8515E+07	4.4216E+08	1.3632E+09	1.5301E+09	1.3584E+09	1.0681E+09
7.5	5.2452E+08	1.7959E+09	5.8649E+09	8.2495E+09	7.1928E+09	4.3528E+09	2.4875E+09	1.2886E+09	5.8925E+08	2.6862E+08	9.4789E+07
8.66	3.0677E+08	1.2340E+09	5.7055E+09	1.3341E+10	1.6520E+10	1.2711E+10	7.8965E+09	3.7982E+09	1.2165E+09	2.3850E+08	0.0000E+00
10	1.3275E+08	6.2670E+08	4.5942E+09	1.6014E+10	2.4316E+10	2.2672E+10	1.7334E+10	1.2520E+10	6.8811E+09	3.3737E+09	9.9201E+08
11.55	5.6565E+07	2.3567E+08	3.0581E+09	1.4633E+10	2.6654E+10	3.0835E+10	2.9228E+10	2.7736E+10	2.0095E+10	1.4551E+10	1.0870E+10
13.34	3.4727E+07	6.9886E+07	1.5972E+09	1.0234E+10	2.3374E+10	3.4548E+10	3.9379E+10	4.4174E+10	3.6685E+10	3.0367E+10	2.6991E+10
15.4	3.6843E+07	3.5937E+07	5.6524E+08	5.2389E+09	1.6797E+10	3.2512E+10	4.3230E+10	5.4576E+10	4.9557E+10	4.4374E+10	4.3245E+10
17.78	4.0198E+07	3.5233E+07	8.4839E+07	1.7772E+09	9.8487E+09	2.5335E+10	3.8672E+10	5.4238E+10	5.3255E+10	5.0999E+10	5.3565E+10
20.54	3.5653E+07	3.4147E+07	9.6713E+06	2.7516E+08	4.4667E+09	1.5950E+10	2.8335E+10	4.4781E+10	4.7955E+10	4.9336E+10	5.5806E+10
23.71	2.9374E+07	3.0594E+07	1.2183E+07	1.3200E+07	1.3736E+09	7.8651E+09	1.7092E+10	3.1447E+10	3.7452E+10	4.1784E+10	5.1014E+10
27.38	2.3983E+07	2.6410E+07	1.4623E+07	0.0000E+00	2.0807E+08	2.7607E+09	8.2119E+09	1.8673E+10	2.5611E+10	3.1473E+10	4.1713E+10
31.62	2.1132E+07	2.3974E+07	2.0195E+07	5.5400E+05	0.0000E+00	4.1518E+08	2.7127E+09	8.8938E+09	1.5117E+10	2.1068E+10	3.0685E+10
36.52	1.9108E+07	2.2229E+07	2.4772E+07	5.7812E+06	2.1906E+05	0.0000E+00	3.9920E+08	3.0376E+09	7.4559E+09	1.2334E+10	2.0060E+10
42.17	1.7787E+07	2.0977E+07	2.5743E+07	1.3139E+07	1.3717E+06	0.0000E+00	4.8531E+06	5.5471E+08	2.9040E+09	6.1099E+09	1.1321E+10
48.7	1.6964E+07	2.0364E+07	2.4142E+07	1.8482E+07	3.9594E+06	2.8749E+03	0.0000E+00	1.4885E+07	7.9167E+08	2.4614E+09	5.2856E+09
56.23	1.6159E+07	1.9880E+07	2.1430E+07	1.9851E+07	8.6922E+06	3.0449E+05	0.0000E+00	0.0000E+00	1.0423E+08	7.1272E+08	1.8674E+09
64.94	1.5150E+07	1.9154E+07	1.8624E+07	1.7536E+07	1.3295E+07	2.3130E+06	3.0443E+04	1.0651E+04	2.5022E+05	1.0540E+08	4.2235E+08
74.99	1.3717E+07	1.7746E+07	1.6120E+07	1.3563E+07	1.4734E+07	6.2042E+06	6.1065E+05	4.5847E+05	1.6711E+05	8.7363E+05	4.0793E+07
86.6	1.2019E+07	1.5529E+07	1.3915E+07	1.0584E+07	1.2805E+07	8.3156E+06	2.3871E+06	1.6934E+06	1.4235E+06	5.3106E+05	5.7179E+05
100	1.0269E+07	1.2882E+07	1.1888E+07	9.2769E+06	9.2796E+06	6.8966E+06	4.0784E+06	2.8713E+06	3.3899E+06	2.3218E+06	1.6567E+06
115.48	8.4443E+06	1.0168E+07	9.7403E+06	8.4867E+06	6.3121E+06	3.4128E+06	3.5377E+06	2.9376E+06	4.2501E+06	6.0977E+06	1.2442E+07
133.35	6.7383E+06	7.9006E+06	7.7398E+06	7.3571E+06	4.8987E+06	1.6487E+06	1.5592E+06	1.8201E+06	3.3650E+06	5.6168E+06	1.2593E+07
153.99	5.1272E+06	6.1343E+06	5.9860E+06	5.7971E+06	4.1981E+06	1.5932E+06	6.7964E+05	9.1820E+05	1.9515E+06	3.1732E+06	7.6787E+06
177.83	3.8563E+06	4.7735E+06	4.5158E+06	4.2334E+06	3.6495E+06	2.2752E+06	1.0071E+06	7.6337E+05	1.0480E+06	1.3090E+06	2.8441E+06
205.35	3.0326E+06	3.6819E+06	3.4085E+06	3.0379E+06	3.0647E+06	2.7943E+06	1.8837E+06	1.4296E+06	1.0977E+06	5.7207E+05	4.9366E+05
237.14	2.4397E+06	2.8185E+06	2.7002E+06	2.2414E+06	2.3979E+06	2.7075E+06	2.2910E+06	1.9769E+06	1.5503E+06	8.4470E+05	2.5881E+05
273.84	2.0208E+06	2.2294E+06	2.2290E+06	1.7470E+06	1.8018E+06	2.1824E+06	2.0682E+06	2.0411E+06	1.8949E+06	1.2900E+06	4.5797E+05
316.23	1.7379E+06	1.8907E+06	1.9275E+06	1.4825E+06	1.4008E+06	1.5663E+06	1.5431E+06	1.6945E+06	1.8863E+06	1.5290E+06	7.7538E+05
365.17	1.4938E+06	1.6776E+06	1.6608E+06	1.3123E+06	1.1206E+06	1.0787E+06	1.0353E+06	1.2486E+06	1.5554E+06	1.4369E+06	9.5144E+05
421.7	1.2503E+06	1.4510E+06	1.3726E+06	1.1282E+06	9.2349E+05	7.7698E+05	7.0093E+05	8.8964E+05	1.1197E+06	1.1228E+06	8.6756E+05
486.97	1.0016E+06	1.1770E+06	1.0707E+06	9.1501E+05	7.6668E+05	5.9049E+05	5.2543E+05	6.3403E+05	7.4414E+05	7.7129E+05	6.5621E+05
562.34	7.8389E+05	9.2930E+05	7.9347E+05	7.1042E+05	6.1703E+05	4.8467E+05	4.4423E+05	4.6355E+05	5.0024E+05	5.0955E+05	4.6263E+05
649.38	6.3316E+05	7.7443E+05	6.0858E+05	5.6144E+05	4.8725E+05	4.1476E+05	4.2466E+05	3.8631E+05	3.8907E+05	3.5986E+05	3.4896E+05
749.89	5.6102E+05	7.0715E+05	5.1377E+05	4.8175E+05	4.0947E+05	3.8239E+05	4.1748E+05	3.6842E+05	3.7577E+05	3.0499E+05	2.9442E+05
865.96	5.3537E+05	6.9608E+05	4.9433E+05	4.4363E+05	3.9068E+05	3.7765E+05	4.0263E+05	3.6900E+05	4.1055E+05	3.1322E+05	2.7088E+05
1000	5.4094E+05	7.1317E+05	5.3761E+05	4.6097E+05	4.2237E+05	3.9777E+05	4.0116E+05	3.8869E+05	4.6441E+05	3.6184E+05	2.6365E+05

	HAB (mm)										
D_p (nm)	21	22	23	24	25	26	27	28	29	30	31
4.87	1.3133E+08	9.9694E+07	7.5984E+07	5.0252E+07	5.5741E+07	6.0435E+07	4.2542E+07	4.5075E+07	4.6246E+07	5.7588E+07	6.2893E+07
5.62	5.2779E+08	3.2451E+08	1.6726E+08	8.8019E+07	7.0259E+07	8.8786E+07	7.5217E+07	5.7989E+07	6.0008E+07	7.4346E+07	6.8968E+07
6.49	7.2521E+08	4.8123E+08	2.5025E+08	1.2791E+08	8.7740E+07	1.1280E+08	9.8208E+07	6.2557E+07	6.8038E+07	8.2186E+07	6.7275E+07
7.5	1.0503E+08	1.5439E+08	1.6352E+08	1.2497E+08	8.9460E+07	7.4327E+07	6.0491E+07	4.5627E+07	5.2178E+07	6.7887E+07	6.4432E+07
8.66	0.0000E+00	1.1257E+07	6.0991E+07	1.2492E+08	7.1726E+07	0.0000E+00	0.0000E+00	2.5470E+06	5.4137E+06	1.9714E+07	3.6313E+07
10	2.4875E+08	5.1564E+07	1.6239E+08	1.8209E+08	1.3542E+08	1.3927E+06	0.0000E+00	0.0000E+00	1.1446E+06	6.4940E+05	1.2047E+07
11.55	7.2063E+09	4.7049E+09	2.4832E+09	1.0613E+09	7.8886E+08	6.6592E+08	4.6937E+08	6.4470E+06	1.1590E+06	4.5902E+05	1.1079E+06
13.34	2.0104E+10	1.5388E+10	8.7370E+09	3.8523E+09	2.9196E+09	2.5465E+09	1.8820E+09	4.7774E+08	2.4982E+08	1.8749E+08	7.2501E+07
15.4	3.4995E+10	3.0194E+10	1.9173E+10	9.0243E+09	6.8191E+09	5.3624E+09	3.7267E+09	1.3628E+09	8.6461E+08	8.1336E+08	5.0529E+08
17.78	4.7100E+10	4.5384E+10	3.2368E+10	1.6384E+10	1.2504E+10	8.6699E+09	5.2672E+09	2.0380E+09	1.5365E+09	1.6265E+09	1.3200E+09
20.54	5.3493E+10	5.7034E+10	4.5145E+10	2.4994E+10	1.9888E+10	1.2413E+10	6.3596E+09	1.9346E+09	1.7063E+09	1.9619E+09	1.8914E+09
23.71	5.3359E+10	6.2317E+10	5.4060E+10	3.3483E+10	2.8567E+10	1.6726E+10	7.4049E+09	9.6198E+08	1.0491E+09	1.3459E+09	1.5803E+09
27.38	4.7795E+10	6.0808E+10	5.7381E+10	4.0309E+10	3.7208E+10	2.1383E+10	8.9805E+09	1.5586E+07	1.2599E+08	2.7577E+08	6.3173E+08
31.62	3.8926E+10	5.3925E+10	5.5136E+10	4.4163E+10	4.4033E+10	2.5812E+10	1.1574E+10	4.1538E+08	9.2551E+06	3.6160E+05	0.0000E+00
36.52	2.8689E+10	4.3487E+10	4.8281E+10	4.4606E+10	4.7974E+10	2.9409E+10	1.4848E+10	2.5976E+09	1.1663E+09	6.6837E+08	2.5037E+08
42.17	1.8861E+10	3.1654E+10	3.8453E+10	4.1639E+10	4.8268E+10	3.1580E+10	1.8936E+10	6.9897E+09	4.1257E+09	3.6578E+09	2.3685E+09
48.7	1.0883E+10	2.0588E+10	2.7624E+10	3.5631E+10	4.4516E+10	3.1807E+10	2.3343E+10	1.4031E+10	9.6502E+09	9.5191E+09	7.0208E+09
56.23	5.3568E+09	1.1753E+10	1.7681E+10	2.7719E+10	3.7355E+10	2.9796E+10	2.6897E+10	2.2302E+10	1.6916E+10	1.7545E+10	1.3848E+10
64.94	2.1607E+09	5.7048E+09	9.8538E+09	1.9343E+10	2.8216E+10	2.5733E+10	2.8371E+10	2.9495E+10	2.4079E+10	2.5800E+10	2.1364E+10
74.99	6.8520E+08	2.2296E+09	4.6174E+09	1.1881E+10	1.8875E+10	2.0235E+10	2.6967E+10	3.3303E+10	2.8990E+10	3.1918E+10	2.7537E+10
86.6	1.7049E+08	6.3088E+08	1.7106E+09	6.2369E+09	1.0906E+10	1.4258E+10	2.2745E+10	3.2356E+10	2.9981E+10	3.3883E+10	3.0411E+10
100	2.6132E+07	1.0560E+08	4.3897E+08	2.6537E+09	5.2158E+09	8.8036E+09	1.6694E+10	2.6931E+10	2.6663E+10	3.0976E+10	2.8979E+10
115.48	2.0688E+07	2.2617E+07	5.6141E+07	8.1936E+08	1.8944E+09	4.5999E+09	1.0344E+10	1.8882E+10	2.0165E+10	2.4186E+10	2.3710E+10
133.35	2.9169E+07	4.5834E+07	2.0651E+07	1.3490E+08	4.1246E+08	1.9100E+09	5.1219E+09	1.0749E+10	1.2617E+10	1.5767E+10	1.6364E+10
153.99	2.4889E+07	5.2959E+07	4.8567E+07	1.3301E+07	5.6616E+06	5.5672E+08	1.8002E+09	4.5802E+09	6.1402E+09	8.1720E+09	9.1665E+09
177.83	1.3326E+07	3.5112E+07	5.1712E+07	1.7073E+07	1.6249E+06	9.0055E+07	3.1456E+08	1.1702E+09	1.9960E+09	3.0154E+09	3.8259E+09
205.35	4.1698E+06	1.3650E+07	3.1646E+07	3.1449E+07	1.9872E+07	1.0629E+07	4.1991E+05	3.5167E+07	2.1535E+08	5.5601E+08	9.3033E+08
237.14	6.0168E+05	2.5517E+06	1.0987E+07	3.1493E+07	3.4884E+07	1.3596E+07	4.7576E+06	0.0000E+00	0.0000E+00	0.0000E+00	0.0000E+00
273.84	1.6408E+05	1.4083E+05	1.3492E+06	2.0969E+07	2.9698E+07	1.4482E+07	6.3374E+06	0.0000E+00	0.0000E+00	0.0000E+00	0.0000E+00
316.23	3.9964E+05	1.4872E+05	2.8510E+04	9.4533E+06	1.6866E+07	1.1016E+07	5.4831E+06	0.0000E+00	0.0000E+00	0.0000E+00	0.0000E+00
365.17	6.8955E+05	4.4208E+05	8.3476E+04	2.0576E+06	5.9061E+06	6.8522E+06	3.2780E+06	0.0000E+00	0.0000E+00	0.0000E+00	0.0000E+00
421.7	8.3731E+05	6.9570E+05	2.0203E+05	7.1521E+04	1.1128E+06	3.4212E+06	1.7287E+06	0.0000E+00	0.0000E+00	0.0000E+00	0.0000E+00
486.97	7.7577E+05	7.7569E+05	3.1363E+05	1.0347E+05	0.0000E+00	1.0643E+06	9.1837E+05	0.0000E+00	0.0000E+00	0.0000E+00	0.0000E+00
562.34	5.9812E+05	7.0160E+05	3.9805E+05	1.2780E+05	0.0000E+00	1.3001E+05	5.1844E+05	0.0000E+00	4.0003E+03	2.2047E+03	9.3749E+02
649.38	4.2548E+05	5.8513E+05	4.6399E+05	1.8103E+05	3.0564E+04	7.2078E+04	0.0000E+00	0.0000E+00	1.8179E+04	9.2317E+03	3.4947E+03
749.89	3.1587E+05	4.9514E+05	4.9747E+05	2.8982E+05	1.2518E+05	1.6328E+05	6.0814E+03	0.0000E+00	0.0000E+00	0.0000E+00	5.1217E+03
865.96	2.7144E+05	4.4068E+05	4.8439E+05	4.1074E+05	2.8700E+05	2.5077E+05	6.9869E+04	0.0000E+00	0.0000E+00	0.0000E+00	0.0000E+00
1000	2.9436E+05	4.3541E+05	4.3983E+05	5.0150E+05	4.2435E+05	3.6012E+05	2.0093E+05	0.0000E+00	0.0000E+00	0.0000E+00	0.0000E+00

	HAB (mm)								
D_p (nm)	32	33	34	35	36	37	38	39	40
4.87	3.4800E+07	4.3998E+07	3.9811E+07	4.1724E+07	3.5658E+07	4.6150E+07	4.1966E+07	3.9801E+07	4.8489E+07
5.62	3.3757E+07	4.4332E+07	4.0523E+07	4.4712E+07	3.7395E+07	4.9560E+07	4.3380E+07	4.4679E+07	5.8404E+07
6.49	3.4307E+07	3.8971E+07	3.9692E+07	4.2553E+07	3.8146E+07	4.7005E+07	4.1350E+07	4.7830E+07	5.5778E+07
7.5	4.3233E+07	4.7383E+07	5.0027E+07	5.1504E+07	4.6543E+07	5.4652E+07	4.8050E+07	4.9242E+07	5.0868E+07
8.66	3.0522E+07	3.6163E+07	3.9403E+07	4.4165E+07	3.6140E+07	4.4026E+07	4.0013E+07	3.5964E+07	3.2602E+07
10	1.5093E+07	2.3046E+07	2.5267E+07	3.3129E+07	2.5563E+07	3.1470E+07	2.9028E+07	2.4628E+07	2.1260E+07
11.55	1.6403E+06	1.9990E+06	2.8680E+06	9.0176E+06	5.6362E+06	7.7117E+06	8.0653E+06	1.1142E+07	2.2528E+07
13.34	6.3277E+06	5.7645E+05	1.7856E+04	7.6759E+04	0.0000E+00	6.3081E+05	2.3667E+06	2.0964E+07	8.4704E+07
15.4	2.2185E+08	1.1398E+08	6.8910E+07	4.8805E+07	2.6274E+07	4.5602E+07	7.7978E+07	1.6039E+08	2.7691E+08
17.78	8.1678E+08	6.3638E+08	5.0907E+08	4.2259E+08	3.7354E+08	4.1240E+08	4.0785E+08	4.8254E+08	5.5584E+08
20.54	1.3190E+09	1.1200E+09	9.4082E+08	8.1558E+08	7.6108E+08	8.0853E+08	7.3427E+08	7.4474E+08	7.2263E+08
23.71	1.1991E+09	1.0664E+09	9.2912E+08	8.4097E+08	8.1547E+08	8.5097E+08	7.3404E+08	6.7853E+08	6.0826E+08
27.38	5.6099E+08	5.3481E+08	5.0200E+08	4.9435E+08	5.1094E+08	5.2174E+08	4.1784E+08	3.4485E+08	3.3041E+08
31.62	0.0000E+00	0.0000E+00	3.4157E+07	8.0688E+07	1.1358E+08	1.0958E+08	6.8549E+07	6.2819E+07	2.0311E+08
36.52	6.5091E+07	0.0000E+00	0.0000E+00	0.0000E+00	0.0000E+00	4.7566E+05	1.9078E+07	1.2427E+08	4.5079E+08
42.17	1.1574E+09	6.2755E+08	4.0187E+08	3.3766E+08	2.5936E+08	3.2433E+08	4.1257E+08	7.4711E+08	1.2376E+09
48.7	4.0383E+09	2.8317E+09	2.1288E+09	1.8158E+09	1.6182E+09	1.7805E+09	1.7728E+09	2.2114E+09	2.6866E+09
56.23	8.7188E+09	6.7939E+09	5.3736E+09	4.6322E+09	4.2827E+09	4.5729E+09	4.2245E+09	4.5091E+09	4.6729E+09
64.94	1.4347E+10	1.1926E+10	9.7067E+09	8.4288E+09	7.9265E+09	8.3460E+09	7.4226E+09	7.2447E+09	6.7977E+09
74.99	1.9510E+10	1.7025E+10	1.4156E+10	1.2365E+10	1.1752E+10	1.2264E+10	1.0642E+10	9.7618E+09	8.5207E+09
86.6	2.2636E+10	2.0596E+10	1.7447E+10	1.5321E+10	1.4676E+10	1.5211E+10	1.2956E+10	1.1317E+10	9.3188E+09
100	2.2657E+10	2.1443E+10	1.8495E+10	1.6322E+10	1.5740E+10	1.6215E+10	1.3597E+10	1.1383E+10	8.9105E+09
115.48	1.9535E+10	1.9242E+10	1.6908E+10	1.4997E+10	1.4552E+10	1.4902E+10	1.2318E+10	9.9094E+09	7.4014E+09
133.35	1.4319E+10	1.4740E+10	1.3222E+10	1.1791E+10	1.1512E+10	1.1713E+10	9.5434E+09	7.3714E+09	5.2548E+09
153.99	8.6595E+09	9.4155E+09	8.6635E+09	7.7742E+09	7.6415E+09	7.7139E+09	6.1812E+09	4.5589E+09	3.0881E+09
177.83	4.0523E+09	4.7795E+09	4.5586E+09	4.1240E+09	4.0872E+09	4.0791E+09	3.1949E+09	2.2162E+09	1.4079E+09
205.35	1.2460E+09	1.7236E+09	1.7480E+09	1.6006E+09	1.6055E+09	1.5704E+09	1.1825E+09	7.4063E+08	4.2529E+08
237.14	1.1643E+08	3.1083E+08	3.6834E+08	3.4533E+08	3.5457E+08	3.2931E+08	2.2273E+08	1.0472E+08	4.7552E+07
273.84	0.0000E+00	0.0000E+00	0.0000E+00	0.0000E+00	0.0000E+00	0.0000E+00	0.0000E+00	0.0000E+00	0.0000E+00
316.23	0.0000E+00	0.0000E+00	0.0000E+00	0.0000E+00	0.0000E+00	0.0000E+00	0.0000E+00	0.0000E+00	0.0000E+00
365.17	0.0000E+00	0.0000E+00	0.0000E+00	0.0000E+00	0.0000E+00	0.0000E+00	0.0000E+00	0.0000E+00	0.0000E+00
421.7	0.0000E+00	0.0000E+00	0.0000E+00	0.0000E+00	0.0000E+00	0.0000E+00	0.0000E+00	0.0000E+00	0.0000E+00
486.97	0.0000E+00	0.0000E+00	0.0000E+00	0.0000E+00	0.0000E+00	0.0000E+00	0.0000E+00	0.0000E+00	1.3017E+03
562.34	0.0000E+00	0.0000E+00	0.0000E+00	0.0000E+00	0.0000E+00	0.0000E+00	0.0000E+00	2.9631E+03	8.6206E+03
649.38	8.9065E+03	0.0000E+00	0.0000E+00	0.0000E+00	0.0000E+00	5.7165E+03	1.0168E+03	1.6885E+04	7.1090E+04
749.89	4.1789E+04	2.9729E+04	9.3398E+04	1.6018E+05	1.0539E+05	1.4478E+05	1.0854E+05	1.2037E+05	1.8310E+05
865.96	4.5519E+03	1.3421E+04	1.4130E+05	2.0247E+05	1.4655E+05	1.7427E+05	1.3556E+05	1.0842E+05	1.0708E+05
1000	0.0000E+00	0.0000E+00	0.0000E+00	0.0000E+00	0.0000E+00	0.0000E+00	0.0000E+00	0.0000E+00	0.0000E+00

Table S4: Averaged measured soot particle size distributions along the centreline of the 15 mol% toluene/heptane flame in dN/dlogD_p (cm^{-3}).

	HAB (mm)										
D_p (nm)	8	9	10	11	12	13	14	15	16	17	18
4.87	8.2456E+07	4.4206E+08	8.7275E+08	6.5531E+08	2.3429E+08	2.1556E+08	3.1163E+08	3.8764E+08	3.5639E+08	2.6052E+08	2.2076E+08
5.62	9.7223E+07	8.7204E+08	2.2027E+09	2.0061E+09	5.2932E+08	1.5250E+08	7.1802E+08	1.2977E+09	1.4443E+09	1.0771E+09	9.1938E+08
6.49	8.3396E+07	1.0641E+09	3.4914E+09	4.3090E+09	2.3594E+09	5.0034E+08	9.6318E+08	1.5626E+09	1.7419E+09	1.3229E+09	1.1768E+09
7.5	7.2561E+07	9.3145E+08	4.2611E+09	8.9153E+09	8.3299E+09	5.1231E+09	2.2978E+09	9.4335E+08	3.3567E+08	1.7087E+08	1.1827E+08
8.66	4.6974E+07	5.7856E+08	4.3033E+09	1.4456E+10	1.6842E+10	1.3992E+10	6.8655E+09	2.5645E+09	2.0840E+08	6.9810E+06	2.1471E+07
10	3.7593E+07	2.5350E+08	3.6717E+09	1.8215E+10	2.4050E+10	2.4812E+10	1.6630E+10	9.9490E+09	4.5543E+09	2.6737E+09	1.4868E+09
11.55	3.8594E+07	1.0149E+08	2.6022E+09	1.8267E+10	2.6770E+10	3.4211E+10	3.0830E+10	2.5348E+10	1.8384E+10	1.4004E+10	1.2372E+10
13.34	3.6098E+07	6.5413E+07	1.4376E+09	1.4990E+10	2.4625E+10	3.9169E+10	4.4508E+10	4.3734E+10	3.7295E+10	3.1366E+10	3.0366E+10
15.4	3.6822E+07	5.9563E+07	5.3572E+08	1.0151E+10	1.9177E+10	3.7860E+10	5.1558E+10	5.7066E+10	5.3405E+10	4.7887E+10	4.8771E+10
17.78	3.7144E+07	5.7291E+07	1.0181E+08	5.6446E+09	1.2665E+10	3.0544E+10	4.8535E+10	5.9470E+10	6.0175E+10	5.7058E+10	6.0738E+10
20.54	3.3259E+07	5.1334E+07	4.5234E+07	2.4693E+09	6.9338E+09	2.0257E+10	3.7816E+10	5.1748E+10	5.6928E+10	5.7183E+10	6.3708E+10
23.71	2.8073E+07	4.4530E+07	4.5719E+07	7.2944E+08	3.0453E+09	1.0893E+10	2.4813E+10	3.8800E+10	4.6992E+10	5.0245E+10	5.8711E+10
27.38	2.2758E+07	3.7408E+07	4.0316E+07	6.6865E+07	9.4946E+08	4.5149E+09	1.3556E+10	2.5209E+10	3.4305E+10	3.9392E+10	4.8489E+10
31.62	1.9090E+07	3.1328E+07	3.3002E+07	5.0144E+06	1.0590E+08	1.1862E+09	5.7634E+09	1.3862E+10	2.2010E+10	2.7611E+10	3.6137E+10
36.52	1.6041E+07	2.6134E+07	2.6603E+07	1.1844E+07	5.2344E+05	1.6031E+08	1.7129E+09	6.1891E+09	1.2122E+10	1.7053E+10	2.4061E+10
42.17	1.3910E+07	2.2387E+07	2.2826E+07	1.7059E+07	2.5588E+06	4.4901E+06	3.8061E+08	2.1265E+09	5.4718E+09	8.9848E+09	1.3969E+10
48.7	1.2757E+07	2.0390E+07	2.2187E+07	1.8093E+07	5.4432E+06	1.6598E+04	1.7716E+07	5.8146E+08	1.8921E+09	3.8509E+09	6.8376E+09
56.23	1.1925E+07	1.9408E+07	2.2955E+07	1.5752E+07	8.8100E+06	2.2782E+05	0.0000E+00	7.8935E+07	4.9459E+08	1.2372E+09	2.6473E+09
64.94	1.1256E+07	1.8809E+07	2.3042E+07	1.2298E+07	1.0957E+07	1.7803E+06	0.0000E+00	0.0000E+00	8.2460E+07	3.0487E+08	7.2895E+08
74.99	1.0334E+07	1.7819E+07	2.1211E+07	9.7712E+06	1.0822E+07	5.7643E+06	1.9641E+05	0.0000E+00	0.0000E+00	4.7674E+07	1.4552E+08
86.6	9.2523E+06	1.6199E+07	1.7694E+07	8.6538E+06	9.3505E+06	8.7542E+06	1.8719E+06	3.5543E+05	6.1624E+03	7.9356E+05	1.5726E+07
100	7.9866E+06	1.3989E+07	1.4030E+07	8.1526E+06	7.3605E+06	7.8376E+06	3.9014E+06	2.1189E+06	1.4006E+06	1.6163E+06	9.7822E+05
115.48	6.7246E+06	1.1445E+07	1.1226E+07	7.3909E+06	5.6493E+06	4.0445E+06	3.7595E+06	3.9660E+06	3.3327E+06	4.0024E+06	8.5725E+06
133.35	5.5399E+06	9.6509E+06	9.0013E+06	6.3330E+06	4.8387E+06	1.7156E+06	1.5235E+06	4.7899E+06	3.9168E+06	4.1959E+06	1.0492E+07
153.99	4.4183E+06	8.1336E+06	6.8133E+06	5.0517E+06	4.1423E+06	1.7903E+06	2.5187E+05	4.0443E+06	2.9491E+06	2.7381E+06	6.5357E+06
177.83	3.3749E+06	6.5224E+06	4.9643E+06	3.7292E+06	3.3383E+06	2.6515E+06	6.6007E+05	3.3985E+06	1.2012E+06	1.2423E+06	2.4253E+06
205.35	2.4564E+06	4.8841E+06	3.6231E+06	2.6498E+06	2.5293E+06	3.1950E+06	1.7798E+06	2.9091E+06	4.6211E+05	3.1702E+05	4.6378E+05
237.14	1.7947E+06	3.5106E+06	2.7900E+06	1.9549E+06	1.8837E+06	2.9599E+06	2.4991E+06	2.4385E+06	6.0745E+05	2.6376E+05	1.7069E+05
273.84	1.3769E+06	2.5855E+06	2.3416E+06	1.5693E+06	1.4526E+06	2.2589E+06	2.4105E+06	2.0343E+06	1.0972E+06	5.4424E+05	2.5995E+05
316.23	1.1474E+06	2.0588E+06	2.0620E+06	1.3398E+06	1.1711E+06	1.5362E+06	1.8506E+06	1.6927E+06	1.4029E+06	8.3498E+05	5.6613E+05
365.17	9.6141E+05	1.7171E+06	1.7760E+06	1.1272E+06	9.6283E+05	1.0233E+06	1.2252E+06	1.3500E+06	1.3301E+06	8.9683E+05	7.6408E+05
421.7	7.5904E+05	1.3583E+06	1.4195E+06	8.9513E+05	7.8768E+05	7.3102E+05	7.5247E+05	9.5262E+05	1.0230E+06	7.5688E+05	7.3901E+05
486.97	5.7231E+05	1.0178E+06	1.0258E+06	6.7897E+05	6.4336E+05	5.7916E+05	4.8412E+05	6.2181E+05	7.0272E+05	5.4810E+05	5.7767E+05
562.34	4.4616E+05	7.3550E+05	6.9540E+05	5.2367E+05	5.3220E+05	5.0074E+05	3.4408E+05	4.0802E+05	4.6981E+05	3.7229E+05	4.0909E+05
649.38	3.8303E+05	5.5797E+05	4.8416E+05	4.3717E+05	4.6649E+05	4.4620E+05	2.9414E+05	3.0404E+05	3.2980E+05	2.6339E+05	2.8149E+05
749.89	4.7031E+05	4.8155E+05	4.1165E+05	4.1429E+05	4.4319E+05	4.2202E+05	3.1853E+05	2.8367E+05	2.6473E+05	2.1841E+05	2.0743E+05
865.96	5.8054E+05	4.9659E+05	4.3972E+05	4.2304E+05	4.4020E+05	4.2565E+05	3.5134E+05	3.0375E+05	2.5787E+05	2.1649E+05	1.8834E+05
1000	6.4573E+05	5.9256E+05	5.6259E+05	4.4973E+05	4.4451E+05	4.5134E+05	3.9083E+05	3.6149E+05	2.9020E+05	2.4168E+05	2.1607E+05

	HAB (mm)										
D_p (nm)	19	20	21	22	23	24	25	26	27	28	29
4.87	1.8470E+08	1.5697E+08	1.0752E+08	6.1451E+07	4.6016E+07	4.9652E+07	3.9253E+07	2.6039E+07	2.9095E+07	2.4942E+07	2.2282E+07
5.62	7.3670E+08	5.6670E+08	3.1441E+08	1.6509E+08	8.0677E+07	6.4549E+07	5.1555E+07	3.9869E+07	4.9756E+07	2.7666E+07	2.7109E+07
6.49	9.7527E+08	7.4329E+08	4.3962E+08	2.6684E+08	1.2555E+08	7.3990E+07	5.7244E+07	5.1884E+07	6.0866E+07	3.2579E+07	3.2853E+07
7.5	1.1267E+08	1.2114E+08	1.7080E+08	1.5460E+08	1.1659E+08	8.4604E+07	4.8886E+07	2.8189E+07	3.2171E+07	2.5873E+07	2.7200E+07
8.66	0.0000E+00	0.0000E+00	1.0151E+07	0.0000E+00	7.5149E+07	9.6043E+07	2.5908E+07	1.2968E+05	5.6804E+05	0.0000E+00	4.8999E+06
10	6.6538E+08	5.0761E+08	3.3447E+07	2.1121E+05	8.7817E+07	1.6479E+08	8.4208E+07	1.1840E+07	8.1615E+06	0.0000E+00	0.0000E+00
11.55	9.8721E+09	7.5214E+09	3.8886E+09	2.4012E+09	1.1403E+09	7.0472E+08	6.4721E+08	5.3018E+08	4.4830E+08	2.0409E+07	0.0000E+00
13.34	2.6261E+10	2.1071E+10	1.2845E+10	8.6928E+09	4.3950E+09	2.5424E+09	2.6446E+09	2.0276E+09	1.7800E+09	7.3880E+08	1.8442E+08
15.4	4.4326E+10	3.7360E+10	2.5856E+10	1.8815E+10	1.0650E+10	6.5277E+09	6.4424E+09	4.2260E+09	3.2606E+09	1.8709E+09	8.1331E+08
17.78	5.7847E+10	5.1359E+10	4.0249E+10	3.1193E+10	1.9754E+10	1.3154E+10	1.1966E+10	6.3206E+09	4.0575E+09	2.5806E+09	1.4955E+09
20.54	6.3662E+10	5.9588E+10	5.2593E+10	4.2894E+10	3.0096E+10	2.2137E+10	1.9340E+10	8.4700E+09	4.0886E+09	2.4054E+09	1.6630E+09
23.71	6.1577E+10	6.0675E+10	5.9934E+10	5.0902E+10	3.9385E+10	3.2419E+10	2.8505E+10	1.1438E+10	4.0560E+09	1.4100E+09	9.8720E+08
27.38	5.3483E+10	5.5475E+10	6.1202E+10	5.3746E+10	4.5700E+10	4.2066E+10	3.8254E+10	1.5633E+10	5.2845E+09	7.0712E+08	0.0000E+00
31.62	4.2160E+10	4.6163E+10	5.6989E+10	5.1503E+10	4.7925E+10	4.8950E+10	4.6679E+10	2.0875E+10	8.2996E+09	1.8378E+09	0.0000E+00
36.52	2.9968E+10	3.4850E+10	4.8606E+10	4.5085E+10	4.6014E+10	5.2031E+10	5.2462E+10	2.6477E+10	1.3767E+10	5.2039E+09	9.3073E+08
42.17	1.8878E+10	2.3583E+10	3.7852E+10	3.5984E+10	4.0527E+10	5.0761E+10	5.4512E+10	3.1538E+10	2.1286E+10	1.1149E+10	4.3198E+09
48.7	1.0320E+10	1.4111E+10	2.6697E+10	2.5970E+10	3.2452E+10	4.5083E+10	5.2079E+10	3.5074E+10	3.0012E+10	1.9832E+10	1.0965E+10
56.23	4.7154E+09	7.2929E+09	1.6848E+10	1.6751E+10	2.3401E+10	3.6194E+10	4.5483E+10	3.6005E+10	3.7822E+10	2.9608E+10	2.0144E+10
64.94	1.7004E+09	3.1438E+09	9.3150E+09	9.4490E+09	1.4938E+10	2.5954E+10	3.6029E+10	3.3813E+10	4.2446E+10	3.7900E+10	2.9688E+10
74.99	4.5041E+08	1.0830E+09	4.3760E+09	4.5174E+09	8.2443E+09	1.6341E+10	2.5578E+10	2.8700E+10	4.2254E+10	4.2161E+10	3.6883E+10
86.6	7.0704E+07	2.5916E+08	1.6652E+09	1.7380E+09	3.7839E+09	8.7927E+09	1.5991E+10	2.1687E+10	3.7042E+10	4.0901E+10	3.9389E+10
100	2.0235E+06	3.3698E+07	4.7463E+08	4.8857E+08	1.3359E+09	3.8509E+09	8.5614E+09	1.4282E+10	2.8228E+10	3.4439E+10	3.6323E+10
115.48	1.9136E+07	2.0991E+07	9.6368E+07	8.6924E+07	2.9565E+08	1.2382E+09	3.7338E+09	7.9129E+09	1.8269E+10	2.4818E+10	2.8730E+10
133.35	2.6886E+07	3.6965E+07	3.8353E+07	2.8368E+07	1.4626E+07	2.1555E+08	1.1897E+09	3.4410E+09	9.6094E+09	1.4878E+10	1.9116E+10
153.99	1.8474E+07	3.3189E+07	4.7349E+07	4.1312E+07	1.8112E+07	1.4922E+06	2.0294E+08	9.9311E+08	3.7372E+09	7.0007E+09	1.0260E+10
177.83	6.9825E+06	1.7115E+07	4.3689E+07	4.1554E+07	4.3256E+07	2.3017E+07	2.2444E+06	9.3169E+07	8.1855E+08	2.2633E+09	4.0497E+09
205.35	1.0885E+06	4.2720E+06	2.5932E+07	2.4952E+07	4.4916E+07	4.7927E+07	2.6749E+07	6.6676E+05	0.0000E+00	3.2365E+08	8.9893E+08
237.14	1.2119E+05	3.7116E+05	1.0178E+07	8.6581E+06	2.7266E+07	4.9167E+07	4.2828E+07	7.4991E+06	0.0000E+00	0.0000E+00	0.0000E+00
273.84	1.3058E+05	2.4830E+05	2.5447E+06	1.3742E+06	9.7651E+06	3.1059E+07	3.4502E+07	1.3141E+07	0.0000E+00	0.0000E+00	0.0000E+00
316.23	3.6833E+05	5.7966E+05	3.1527E+05	1.1694E+04	1.2458E+06	1.2441E+07	1.7560E+07	1.2113E+07	1.8114E+05	0.0000E+00	0.0000E+00
365.17	6.9546E+05	1.0022E+06	6.4351E+05	3.0660E+04	1.3630E+02	2.6029E+06	4.4601E+06	8.0801E+06	6.0711E+05	0.0000E+00	0.0000E+00
421.7	8.2322E+05	1.1605E+06	8.9027E+05	1.0676E+05	9.9044E+03	3.1684E+05	1.0554E+05	4.1734E+06	1.2394E+06	0.0000E+00	0.0000E+00
486.97	7.2595E+05	1.0234E+06	8.9375E+05	2.0799E+05	2.3494E+04	2.0219E+04	0.0000E+00	1.7252E+06	1.2995E+06	0.0000E+00	0.0000E+00
562.34	5.3061E+05	7.3831E+05	7.3623E+05	2.8300E+05	4.6758E+04	2.8262E+04	0.0000E+00	5.1386E+05	6.8316E+05	1.0619E+04	0.0000E+00
649.38	3.7291E+05	4.6800E+05	5.6716E+05	3.3198E+05	1.0461E+05	7.1193E+04	1.3621E+04	0.0000E+00	0.0000E+00	0.0000E+00	0.0000E+00
749.89	3.0926E+05	3.2281E+05	4.6909E+05	3.5000E+05	1.8639E+05	1.5844E+05	6.1510E+04	7.3580E+03	0.0000E+00	0.0000E+00	0.0000E+00
865.96	3.0860E+05	2.9635E+05	4.4588E+05	3.4055E+05	2.5285E+05	2.7253E+05	1.5380E+05	4.5118E+04	0.0000E+00	0.0000E+00	0.0000E+00
1000	3.3062E+05	3.7784E+05	4.7212E+05	3.1789E+05	2.6900E+05	3.4515E+05	2.5644E+05	9.9543E+04	0.0000E+00	0.0000E+00	0.0000E+00

	HAB (mm)										
D_p (nm)	30	31	32	33	34	35	36	37	38	39	40
4.87	3.4612E+07	4.0826E+07	3.1626E+08	3.0786E+07	2.5566E+07	3.4918E+07	2.4073E+07	2.4962E+07	3.8550E+07	4.9787E+07	2.5571E+07
5.62	3.9234E+07	4.3757E+07	3.8220E+08	2.7498E+07	2.0697E+07	3.5369E+07	2.3468E+07	2.4314E+07	3.9421E+07	5.6610E+07	2.8285E+07
6.49	3.7085E+07	3.4780E+07	2.6537E+08	1.7397E+07	1.3462E+07	2.7934E+07	1.9511E+07	2.0381E+07	3.3497E+07	4.9292E+07	2.6878E+07
7.5	3.5389E+07	2.6481E+07	1.9011E+08	2.2391E+07	1.9198E+07	2.9438E+07	2.5391E+07	2.6114E+07	3.8704E+07	4.8470E+07	2.8747E+07
8.66	1.9064E+07	1.5201E+07	2.0196E+08	2.0689E+07	1.6081E+07	2.7621E+07	2.5186E+07	2.5468E+07	3.2358E+07	4.9429E+07	2.2236E+07
10	3.7670E+06	7.4216E+06	2.1370E+08	1.6101E+07	1.3371E+07	2.5147E+07	2.4890E+07	2.3266E+07	2.3228E+07	5.3355E+07	1.6759E+07
11.55	0.0000E+00	0.0000E+00	1.6540E+08	1.4589E+06	2.9956E+06	8.4409E+06	1.3253E+07	1.0627E+07	8.1681E+06	3.1314E+07	6.5477E+06
13.34	3.0835E+06	0.0000E+00	1.6971E+08	0.0000E+00	0.0000E+00	0.0000E+00	2.7550E+06	0.0000E+00	0.0000E+00	2.6376E+06	6.0777E+05
15.4	2.9736E+08	2.7596E+08	4.4880E+08	1.4088E+07	5.6406E+05	2.6657E+06	1.2017E+06	1.0119E+06	3.6384E+06	9.2794E+06	1.8567E+07
17.78	9.5365E+08	9.7765E+08	1.1277E+09	2.5300E+08	1.8001E+08	1.7919E+08	1.3849E+08	1.2514E+08	1.4981E+08	1.5343E+08	1.5371E+08
20.54	1.4965E+09	1.5855E+09	1.7047E+09	5.1730E+08	4.2641E+08	4.3328E+08	3.5768E+08	3.2188E+08	3.6618E+08	3.6826E+08	3.1681E+08
23.71	1.3539E+09	1.4746E+09	1.5902E+09	5.5757E+08	5.1878E+08	5.4341E+08	4.6842E+08	4.1947E+08	4.6033E+08	4.6329E+08	3.5638E+08
27.38	6.1646E+08	7.1271E+08	8.6089E+08	3.4866E+08	3.9081E+08	4.2939E+08	3.8791E+08	3.4517E+08	3.6270E+08	3.6871E+08	2.4498E+08
31.62	0.0000E+00	0.0000E+00	1.2470E+08	7.5894E+07	1.5366E+08	1.8492E+08	1.7861E+08	1.5760E+08	1.5513E+08	1.6109E+08	7.9489E+07
36.52	7.5980E+07	0.0000E+00	2.6040E+07	0.0000E+00	0.0000E+00	0.0000E+00	0.0000E+00	0.0000E+00	9.9615E+05	1.5863E+06	4.1584E+06
42.17	1.7230E+09	1.4296E+09	1.0490E+09	2.6855E+08	1.3957E+08	9.2251E+07	4.2231E+07	4.4712E+07	8.9268E+07	1.0357E+08	2.0990E+08
48.7	5.9578E+09	5.5447E+09	4.3105E+09	1.9810E+09	1.4914E+09	1.3265E+09	9.9746E+08	9.7454E+08	1.1826E+09	1.2423E+09	1.3771E+09
56.23	1.2508E+10	1.2335E+10	1.0011E+10	5.5288E+09	4.4769E+09	4.1801E+09	3.3571E+09	3.2340E+09	3.7500E+09	3.7174E+09	3.6364E+09
64.94	2.0026E+10	2.0587E+10	1.7320E+10	1.0548E+10	8.8454E+09	8.4568E+09	7.0080E+09	6.6969E+09	7.6190E+09	7.2856E+09	6.6850E+09
74.99	2.6567E+10	2.8285E+10	2.4605E+10	1.6001E+10	1.3734E+10	1.3338E+10	1.1275E+10	1.0713E+10	1.2043E+10	1.1227E+10	9.8646E+09
86.6	3.0149E+10	3.3169E+10	2.9829E+10	2.0427E+10	1.7861E+10	1.7559E+10	1.5063E+10	1.4251E+10	1.5871E+10	1.4509E+10	1.2324E+10
100	2.9587E+10	3.3644E+10	3.1329E+10	2.2458E+10	1.9964E+10	1.9835E+10	1.7223E+10	1.6238E+10	1.7940E+10	1.6137E+10	1.3313E+10
115.48	2.5063E+10	2.9530E+10	2.8576E+10	2.1411E+10	1.9341E+10	1.9406E+10	1.7036E+10	1.6017E+10	1.7562E+10	1.5570E+10	1.2501E+10
133.35	1.8082E+10	2.2202E+10	2.2477E+10	1.7640E+10	1.6204E+10	1.6423E+10	1.4572E+10	1.3668E+10	1.4870E+10	1.3000E+10	1.0155E+10
153.99	1.0778E+10	1.3959E+10	1.4976E+10	1.2384E+10	1.1601E+10	1.1896E+10	1.0682E+10	9.9946E+09	1.0777E+10	9.2811E+09	7.0289E+09
177.83	4.9699E+09	6.9807E+09	8.1475E+09	7.1854E+09	6.9112E+09	7.2052E+09	6.5703E+09	6.1290E+09	6.5302E+09	5.5214E+09	4.0178E+09
205.35	1.4962E+09	2.4692E+09	3.3266E+09	3.2020E+09	3.2207E+09	3.4610E+09	3.2353E+09	3.0019E+09	3.1367E+09	2.5840E+09	1.7670E+09
237.14	1.2435E+08	4.1821E+08	8.0233E+08	8.9293E+08	1.0023E+09	1.1626E+09	1.1443E+09	1.0485E+09	1.0519E+09	8.2787E+08	4.9692E+08
273.84	0.0000E+00	0.0000E+00	0.0000E+00	1.7708E+07	9.4227E+07	1.7393E+08	2.0722E+08	1.8048E+08	1.5556E+08	1.0733E+08	3.0603E+07
316.23	0.0000E+00	0.0000E+00	0.0000E+00	0.0000E+00	0.0000E+00	0.0000E+00	0.0000E+00	0.0000E+00	0.0000E+00	0.0000E+00	0.0000E+00
365.17	0.0000E+00	0.0000E+00	0.0000E+00	0.0000E+00	0.0000E+00	0.0000E+00	0.0000E+00	0.0000E+00	0.0000E+00	0.0000E+00	0.0000E+00
421.7	0.0000E+00	0.0000E+00	0.0000E+00	0.0000E+00	0.0000E+00	0.0000E+00	0.0000E+00	0.0000E+00	0.0000E+00	0.0000E+00	0.0000E+00
486.97	0.0000E+00	0.0000E+00	4.1079E+02	0.0000E+00	0.0000E+00	0.0000E+00	0.0000E+00	0.0000E+00	0.0000E+00	0.0000E+00	0.0000E+00
562.34	0.0000E+00	0.0000E+00	2.6604E+06	0.0000E+00	0.0000E+00	0.0000E+00	0.0000E+00	0.0000E+00	0.0000E+00	1.4926E+04	4.8319E+03
649.38	3.5275E+04	1.6845E+05	7.3142E+06	5.2713E+05	3.5978E+05	7.0966E+04	2.6465E+04	1.0577E+05	1.8682E+05	2.8405E+05	2.8696E+05
749.89	1.2216E+05	2.8604E+05	8.5433E+06	1.3372E+06	9.3547E+05	8.6697E+05	6.5404E+05	7.9625E+05	9.0699E+05	1.1055E+06	6.7511E+05
865.96	0.0000E+00	2.0739E+04	5.0166E+06	9.8719E+05	7.2127E+05	8.2212E+05	7.4038E+05	8.5933E+05	9.1650E+05	1.1008E+06	5.2787E+05
1000	0.0000E+00	0.0000E+00	0.0000E+00	0.0000E+00	0.0000E+00	2.5526E+04	2.0156E+05	2.7255E+05	2.3551E+05	3.2713E+05	3.6113E+04

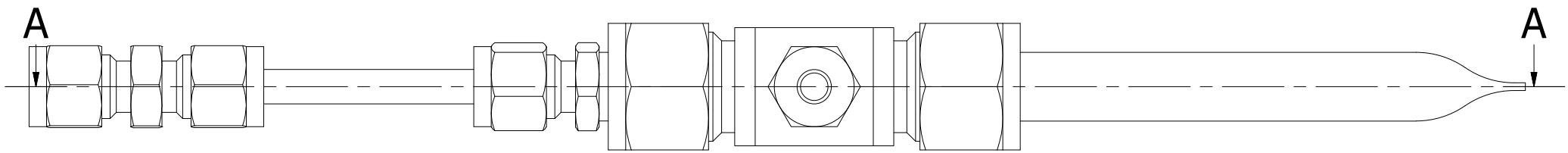

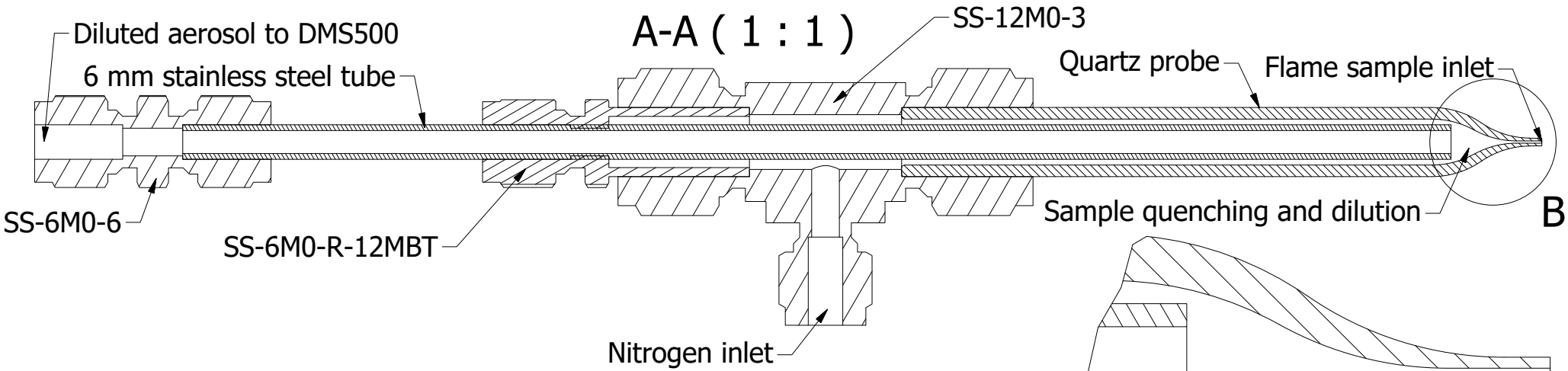

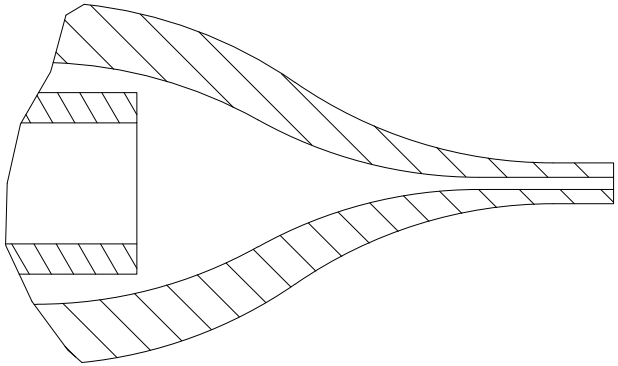

B (4 : 1)

Cite:
J.A.H. Dreyer, M. Poli, N. Eaves, M.L. Botero, J. Akroy, S. Mosbach, M. Kraft, Evolution of the soot particle size distribution along the centreline of a n-heptane/toluene co-flow diffusion flame

Designed by	Checked by	Approved by	Date		Date	
Jochen A.H. Dreyer					16/07/2018	

CoMo group, University of Cambridge	Aerosol sampling probe		
		Edition	Sheet 1 / 1